



Auditory Target Detection Enhances Visual Processing and Hippocampal Functional Connectivity

Roy Moyal¹, Hamid B. Turker¹, Wen-Ming Luh² and Khen M. Swallow^{1*}

¹ Cognitive Science Program, Department of Psychology, Cornell University, Ithaca, NY, United States, ² National Institute on Aging, National Institutes of Health, Baltimore, MD, United States

OPEN ACCESS

Edited by:

Pietro Spataro,
Mercatorum University, Italy

Reviewed by:

Mingzhu Hou,
The University of Texas at Dallas,
United States
Marianne Andrea De Chastelaine,
The University of Texas at Dallas,
United States

*Correspondence:

Khen M. Swallow
kms424@cornell.edu

Specialty section:

This article was submitted to
Cognition,
a section of the journal
Frontiers in Psychology

Received: 08 March 2022

Accepted: 18 May 2022

Published: 13 June 2022

Citation:

Moyal R, Turker HB, Luh W-M and
Swallow KM (2022) Auditory Target
Detection Enhances Visual
Processing and Hippocampal
Functional Connectivity.
Front. Psychol. 13:891682.
doi: 10.3389/fpsyg.2022.891682

Though dividing one's attention between two input streams typically impairs performance, detecting a behaviorally relevant stimulus can sometimes enhance the encoding of unrelated information presented at the same time. Previous research has shown that selection of this kind boosts visual cortical activity and memory for concurrent items. An important unanswered question is whether such effects are reflected in processing quality and functional connectivity in visual regions and in the hippocampus. In this fMRI study, participants were asked to memorize a stream of naturalistic images and press a button only when they heard a predefined target tone (400 or 1,200 Hz, counterbalanced). Images could be presented with a target tone, with a distractor tone, or without a tone. Auditory target detection increased activity throughout the ventral visual cortex but lowered it in the hippocampus. Enhancements in functional connectivity between the ventral visual cortex and the hippocampus were also observed following auditory targets. Multi-voxel pattern classification of image category was more accurate on target tone trials than on distractor and no tone trials in the fusiform gyrus and parahippocampal gyrus. This effect was stronger in visual cortical clusters whose activity was more correlated with the hippocampus on target tone than on distractor tone trials. In agreement with accounts suggesting that subcortical noradrenergic influences play a role in the attentional boost effect, auditory target detection also caused an increase in locus coeruleus activity and phasic pupil responses. These findings outline a network of cortical and subcortical regions that are involved in the selection and processing of information presented at behaviorally relevant moments.

Keywords: attentional boost effect, visual processing, encoding, hippocampus, locus coeruleus, temporal selection

Abbreviations: AC, auditory cortex; ACC, anterior cingulate cortex; AUC, area under the curve; FG, fusiform gyrus; aHPC, anterior hippocampus; pHPC, posterior hippocampus; iFC, intrinsic functional connectivity; IRF, impulse response function; LC, locus coeruleus; MC, motor cortex; ME, multi-echo; ME-ICA, multi-echo independent component analysis; NE, norepinephrine; nmT1, neuromelanin-weighted T1; PG, parahippocampal gyrus; SVM, support vector machine; V1, primary visual cortex; V2, secondary visual cortex.

INTRODUCTION

Attention can be allocated not only to spatial locations or stimulus features (Carrasco, 2011), but also to information presented at particular points in time (Rohenkohl et al., 2011; Nobre and van Ede, 2018). A growing literature shows that perceptual processing is enhanced when events change in meaningful ways (e.g., Jefferies and Di Lollo, 2019) and when they require a response (Swallow and Jiang, 2010; Makovski et al., 2013; Yebra et al., 2019; Clewett et al., 2020). Detecting a behaviorally relevant item, for instance, can improve memory for concurrently presented but otherwise unrelated information (the attentional boost effect, or ABE; Swallow and Jiang, 2010), even when it is task-irrelevant (Swallow and Jiang, 2014; Turker and Swallow, 2019; Broitman and Swallow, 2020). Target detection can also increase visual adaptation, lexical priming, and affective evaluation of concurrently presented items (Pascucci and Turatto, 2013; Spataro et al., 2013; Schonberg et al., 2014; Swallow and Atir, 2019). The beneficial effects of presenting information at the same time as a target can be contrasted with those commonly observed in attention tasks that require participants to select among different sources of information. Under these conditions, competitive interactions within and between regions are associated with reduced processing of unselected information (e.g., in visual cortex when monitoring auditory rather than visual stimuli, Johnson and Zatorre, 2005; of multi-voxel patterns associated with task irrelevant categories when searching for a pre-specified category of objects in natural images, Seidl et al., 2012; in parts of topographically organized visual cortex in uncued regions of a visual display during a search task, Silver et al., 2007). However, despite the extensive evidence that the selection of one item (such as an auditory tone) reliably boosts behavioral indices of background item (such as a visual scene) processing, little is known about its neural basis. Guided by previous empirical work, this project used fMRI to study the neurophysiological basis of the effects of target detection on visual processing and memory in the ABE paradigm. Specifically, we examined whether it enhances the quality of representations in—and communication between—regions involved in episodic encoding.

Consistent with prior work demonstrating that norepinephrine (NE) increases neural gain in response to behaviorally relevant events or task boundaries (Aston-Jones and Cohen, 2005; Bouret and Sara, 2005; Lee et al., 2018), the ABE could reflect the phasic firing of the locus coeruleus (LC) in response to behaviorally relevant events (Swallow and Jiang, 2013). The LC, a brainstem structure whose activity briefly increases in response to changes in a task or in the environment (Sara, 2009; Clewett et al., 2020) and facilitates episodic encoding (Takeuchi et al., 2016), is the main source of NE in the brain. Phasic LC responses correlate with pupil diameter (Murphy et al., 2014; Joshi et al., 2016) and are associated with target detection and orienting (Aston-Jones et al., 1994; Breton-Provencher and Sur, 2019). Though previous studies suggest a relationship between LC activity and the ABE (Swallow et al., 2019; Yebra et al., 2019), they utilized indirect measures (pupil size) or a probabilistic atlas to identify the LC in participants, making it

difficult to pinpoint the source of the modulatory signals (cf. Wang and Munoz, 2015). This is of particular concern because the small size of the LC and its location near the fourth ventricle, a source of physiological noise in fMRI, increase the potential for mislocalization and for the inclusion of spurious signals in estimates of LC activity (Turker et al., 2021). We therefore utilized structural MRI T1 sequences that increase contrast for the high concentrations of neuromelanin in the LC (Keren et al., 2009) to improve our ability to localize the LC in individual participants relative to a probabilistic atlas (Turker et al., 2021). We also employed multi-echo EPI with multi-echo independent components analysis (ME-ICA) and TE-dependent BOLD signal classification (Kundu et al., 2013) to reduce the contributions of noise sources to our data.

The effects of target detection on episodic encoding, visual adaptation, and lexical priming (e.g., Pascucci and Turatto, 2013; Spataro et al., 2013; Turker and Swallow, 2019; Broitman and Swallow, 2020) suggest that it should improve the quality of representations in perceptual and episodic encoding regions. Such effects would also be expected if target detection increases neural gain, enhancing the signal to noise ratio of activity in impacted regions (e.g., Aston-Jones and Cohen, 2005). However, fMRI investigations of the ABE have provided little insight into the mechanisms by which it modulates neural processing. Prior work has shown that target detection broadly increases the BOLD signal in regions not directly involved in processing the target stimulus (e.g., auditory target detection boosts activity in V1; Jack et al., 2006; Swallow et al., 2012). These studies did not include baseline trials, however, making it unclear whether the reported effects reflect target-related facilitation or distractor-related inhibition. Moreover, differences in the magnitude of the hemodynamic response do not, on their own, reflect differences in processing quality (cf. Albers et al., 2018). This study therefore incorporated baseline trials and used multivoxel pattern analysis to test whether target detection enhances the quality of processing (Mahmoudi et al., 2012). Attention-related enhancements in processing quality often coincide with changes in the amount or spread of decodable representational information in perceptual regions (e.g., Zhang et al., 2011); in the medial temporal lobe, increases in BOLD magnitude and decoding accuracy (e.g., Chadwick et al., 2010, 2011) have been linked to episodic encoding and recall. Nonetheless, the relationship between auditory target detection and the quality of visual processing and encoding remains underexplored.

Prior research also leaves the possibility that target detection in the ABE paradigm affects coordination among different brain regions unexplored. Better working memory (Gazzaley et al., 2004) and episodic encoding (Ranganath et al., 2005) are associated with enhanced functional connectivity (Friston, 2011) between the hippocampus (HPC) and visual areas. Findings of enhanced short-term memory (Makovski et al., 2011; Li et al., 2018) and episodic encoding (Leclercq et al., 2014; Turker and Swallow, 2019; Broitman and Swallow, 2020; Mulligan et al., 2021) with the ABE thus suggest that it should increase functional connectivity between these regions. Phasic LC activation also is temporally coordinated with the HPC, anterior cingulate cortex (ACC), and other prefrontal regions (cf. Sara, 2015) and

may lead to the dynamic reconfiguration of cortical functional networks (Bouret and Sara, 2005; Shine et al., 2018; Li et al., 2019). Disruptions to existing population firing patterns created by phasic LC activation could also facilitate the formation of patterns that represent behaviorally relevant information (Moyal and Edelman, 2019). While these findings suggest that auditory target detection should trigger an increase in visuo-hippocampal connectivity, this possibility has yet to be examined directly. It may also be possible that the anterior and posterior hippocampus (aHPC and pHPC, respectively) are differently impacted by target detection. Relative to pHPC, aHPC is more strongly associated with episodic memory encoding (relative to spatial memory encoding), is associated with more generalized (less detailed) representations of events, shows stronger functional connectivity with fusiform gyrus (FG) and medial versus lateral aspects of entorhinal cortex, and may have greater concentrations of NE receptors (Gage and Thompson, 1980; Poppenk et al., 2013; Persson et al., 2018; Frank et al., 2019). However, non-human animal research also suggests that the LC may play a role in modulating episodic memory formation in pHPC (Kempadoo et al., 2016; Wagatsuma et al., 2018). We therefore investigated the effects of auditory target detection in the ABE paradigm on the functional connectivity of aHPC and pHPC to visual areas.

To summarize, we used multi-echo fMRI to characterize the neural correlates of target detection in the ABE, specifically examining responses of the visual cortex, HPC, and LC to images presented on their own or with auditory target or distractor tones (Swallow and Jiang, 2010; Swallow et al., 2012). We expected target detection to increase (1) phasic pupil responses and activity in individually defined LC; (2) the ability to classify patterns of BOLD activity associated with different categories of images; and (3) functional connectivity between visual regions and HPC. We found evidence supporting each of these hypotheses.

MATERIALS AND METHODS

Participants

Twenty-one right-handed individuals (15 female, 6 male, 19–40 years old, $M = 21.48$, $SD = 4.86$) participated in the study. They were screened for non-MRI compatible medical devices or body modifications, claustrophobia, movement disorders, pregnancy, mental illness, use of medication affecting cognition, and color blindness. Consent was obtained at the beginning of the session and participants were debriefed at the end. All procedures were approved by the Cornell University review board. Sample size was based on a previous study examining the effect of auditory target detection on visual cortical activity (Swallow et al., 2012), which reported effect sizes for a peak signal difference following target and distractor auditory tones of $Cohen's f > 1.037$. A sample size of 20 was selected to ensure that smaller effects between conditions and in other measures of connectivity and classification could be detected. With a sample of 20 and false positive rate of 0.05, a traditional one-way (three levels) repeated measures analysis of variance has a power of 0.95 to detect an effect of $Cohen's f > 0.378$ (calculated using G^* Power; Faul et al., 2007).

Two participants responded to the wrong tones on some scans so that some images were paired with both target and distractor tones (one of these participants also did not complete the memory test). Because these participants were performing the target detection task (but with the wrong tone) their data for these scans were recoded and included in analyses of detection task performance and in the univariate analyses (which had an N of 21). However, these two participants were excluded from analyses that depended on balancing the number of trials across conditions (image classification and functional connectivity, which fed into an image classification analysis), resulting in an N of 19 for these analyses. They were also excluded from analyses involving the memory test. One additional participant did not complete the memory test due to a fire alarm, leaving 18 participants for all analyses involving memory data.

MRI and Pupillometry Data Acquisition

Magnetic resonance imaging was performed with a 3T GE Discovery MR750 MRI scanner (GE Healthcare, Milwaukee, WI, United States) and a 32-channel head coil at the Cornell Magnetic Resonance Imaging Facility in Ithaca, NY, United States. Participants laid supine on the scanner bed with their head supported and immobilized. Ear plugs and headphones (MR confon GmbH, Germany) were used to reduce scanner noise, allow the participant to communicate with the experimenters, and present auditory stimuli during the tasks. Visual stimuli were presented with a 32" Nordic Neuro Lab liquid crystal display (1,920 pixels \times 1,080 pixels, 60 Hz, 6.5 ms g to g) located at the head of the scanner bore and viewed through a mirror attached to the head coil.

Anatomical data were acquired with a T1-weighted MPRAGE sequence (TR = 7.7 ms; TE = 3.42 ms; 7° flip angle; 1.0 mm isotropic voxels, 176 slices). A second anatomical scan utilized a neuromelanin sensitive T1-weighted partial volume turbo spin echo (TSE) sequence (TR = 700 ms; TE = 13 ms; 120° flip angle; 0.430 mm \times 0.430 mm in-plane voxels, 10 interleaved 3.0 mm thick axial slices; adapted from Keren et al., 2009). Slices for the TSE volume were oriented perpendicular to the long axis of the brain stem to provide high resolution data in the axial plane, where dimensions of the LC are smallest, and positioned to cover the most anterior portion of the pons. Multi-echo echo planar imaging (EPI) sequences were used to acquire functional data during the four task runs (TR = 2,500 ms; TEs = 12.3, 26.0, and 40.0 ms; 80° flip angle; 3.0 mm isotropic voxels; 44 slices). In addition to the task runs, all participants also completed a single resting state scan with their eyes open and the lights on (612 s; TR = 3.0 s; TEs = 13, 30, and 47 ms; 83° flip angle; 3.0 mm isotropic voxels; 46 slices). Resting state data are reported elsewhere (Turker et al., 2021) but were used for this study (see Section "Locus Coeruleus Functional Connectivity").

During the scans, pupil size and gaze location were acquired using an EyeLink 1000 Plus MRI Compatible eye tracker (SR-Research, Canada) for all but two participants (1,000 Hz, right eye). After the participant was positioned in the scanner, mirrors were adjusted to bring the eye into view of the camera. Immediately prior to the resting state scan, thresholds defining pupil and corneal reflectance were automatically adjusted and

a nine-point calibration routine was performed to determine the parameters needed to estimate gaze position. Calibration was validated and adjusted as necessary prior to each scan that included eye data measurement. On task runs, participants were instructed to fixate the central dot and minimize blinking.

MRI Data Preprocessing

All EPI data were denoised and processed using the standard ME-ICA pipeline, except as indicated (meica.py, Version 3.2, beta 1; Kundu et al., 2012, 2013). First, the MPRAGE volume was skull stripped using FSL v5.0 BET ($b = 0.25$). After matching the obliquity of the anatomical volume and EPI time series, motion was estimated from the first echo time series using 3dvolreg and the third volume as the target. Third, all EPI data were despiked and slice time acquisition differences were corrected using 3dTshift. Fourth, for each echo time series, the first two volumes were dropped and the remaining EPI data were registered to the third volume. Baseline intensity volume (s_0), the t_2^* map volume (t_2^*), and the optimal combination volume time series were then calculated. Fifth, registration and alignment transforms were applied to the EPI data and the pre-equilibrium volumes dropped in one step to align the data with the individual anatomical volume in its original acquisition space. Sixth, EPI data were denoised to identify and separate BOLD components from non-BOLD components (Kundu et al., 2013). BOLD components were recombined to create the denoised data sets that were used in subsequent analyses. Finally, denoised EPI data were spatially aligned to the MNI N27 atlas for volume-wise group level analyses.

Region of Interest Identification

Individual MPRAGE scans were submitted to FreeSurfer's segmentation and surface-based reconstruction software (recon-all v5.3¹; Dale et al., 1999; Fischl et al., 1999) to label voxels according to each individual's anatomy. Labels for the fourth ventricle (4V), hippocampus (HPC), motor cortex (MC), planum temporale for auditory cortex (AC), primary visual cortex (V1), secondary visual cortex (V2), fusiform gyrus (FG), and parahippocampal gyrus (PG) were extracted and converted to volumetric ROIs using FreeSurfer and AFNI tools (Cox, 1996; Cox and Hyde, 1997; Gold et al., 1998). Separate ROIs were created for the left and right hemispheres. In addition, the HPC ROIs were divided into anterior and posterior portions at the anterior-posterior coordinate of their center of mass (aHPC and pHPC), to account for possible differences in their connectivity patterns and function (Fanselow and Dong, 2010; Poppenk et al., 2013). Detailed methods for identifying the LC are described in Turker et al. (2021). Briefly, individual MPRAGE scans (including skull) were aligned to the individual normalized T1-weighted neuromelanin scan. After extracting the brainstem from the nmT1, correcting image intensity, and setting the false color palette to the predefined range, candidate LC voxels could be visually distinguished from nearby regions (**Figure 3A** and **Supplementary Figure 3**). Bilateral LC ROIs were then hand-drawn by two tracers (voxel size: 0.43 mm \times 0.43 mm \times 3.0 mm).

¹surfer.nmr.mgh.harvard.edu

Voxels included as LC by both raters were kept, resampled to 3 mm isotropic voxels, and spatially aligned to the individual EPI and MPRAGE. This procedure resulted in an average of 4.5 voxels per participant ($SD = 1.9$). Finally, we also created an ROI for the ACC, based on its connections with the LC (e.g., Ennis et al., 1998). The association test map for the ACC was downloaded from Neurosynth² and thresholded ($z = 6$) to retain an ROI covering only putative ACC.

Experimental Design and Statistical Analysis

Stimuli

Two hundred eighty-eight full color images of faces (48 female and 48 male), objects (48 cars and 48 chairs), and outdoor scenes (48 beaches and 48 forests) were acquired from personal collections and publicly available online databases³ (Huang et al., 2007; Huang and Learned-Miller, 2014; Xiang et al., 2014). 24 images from each subcategory were used in the encoding task (eight in each tone type condition), each presented once per run (four repetitions in total). The rest of the images were used as foils in the recognition test. Scrambled images were generated from these photographs by dividing them into 32×32 tiles and shuffling their locations. The mean and variance of pixel intensity (luminance) was matched across images using the SHINE toolbox (Willenbockel et al., 2010). The presentation of simple auditory stimuli with complex naturalistic images is standard for this paradigm (e.g., Swallow and Jiang, 2010, 2012; Swallow et al., 2012, 2019) and allows for the separation of the effects of selection on processing the target and distractor tones from the impact of auditory target detection on visual stimuli processing.

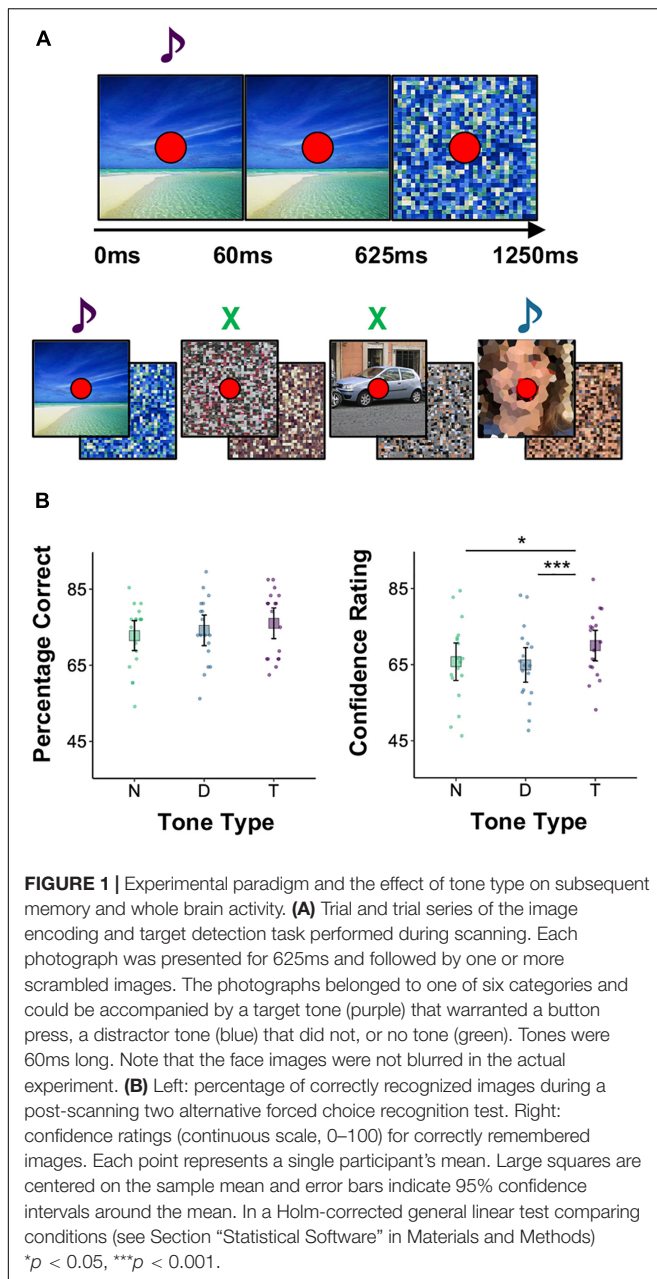
Design and Procedure

In the four functional runs (407.5 s each) participants continuously performed simultaneous image encoding and target detection tasks. On each 1.25 s long trial, one image (7×7 visual degrees; 256 pixels \times 256 pixels) was presented for 625 ms and immediately followed by another image for another 625 ms. On most trials, both images were scrambled (no-task trials, 164/run). On task trials (144/run), the first image was a photograph and the second was a scrambled version of that photograph. Participants attempted to memorize the photograph for a later memory test. The inter-trial interval was 0 ms, ensuring that there was an image on the screen throughout the task and that it changed every 625 ms (**Figure 1A**). A red fixation dot (0.25 visual degree diameter) appeared at the center of the screen throughout the task, including 7.5 s of pre-task fixation and 15 s of post-task fixation at the beginning and end of each run, respectively. Scrambled images (alternating every 625 ms) were presented during the pre- and post-task fixation periods as well to avoid large visual transients at the onset and offset of the task.

On some task trials a high (1,200 Hz) or low (400 Hz) pitched auditory tone (60 ms duration) was played over the headphones at the same time an image was presented (0 ms stimulus onset asynchrony). If the tone was the pre-specified target pitch

²neurosynth.org

³vision.stanford.edu/projects/sceneclassification/resources.html



participants pressed a button with their right thumb. Participants made no overt response if the tone was not the pre-specified target pitch (distractor) or if no tone was presented on that trial. The tone assigned to the target condition was counterbalanced within participants by switching it halfway through the encoding task (e.g., high, high, low, and low). Participants were told which tone was the target tone at the beginning of each run. The starting target tone was counterbalanced across participants: Half started with the high tone as the target and half started with the low tone as the target. Tone condition (target, distractor, and no tone) was held constant for each image. Thus, if a high tone was assigned to a given image on the first two runs, it was switched to a low tone on the latter two runs. An equal number of task trials was assigned to each tone type (target, distractor, and no

tone), ensuring that results cannot be attributed to the salience or relative frequency of target occurrences. Tones were never presented on no-task trials. Sound levels were adjusted during the MPRAGE scan to ensure participants could hear both tones during scanning. Participants practiced the task with a different set of images before entering the scanner.

After scanning, participants completed a two alternative forced choice recognition test on the images. On each trial, two images were presented on the screen, one on the left side and one on the right. One of the images was presented during the encoding and detection task and the other was a new image (the location of the old image was pseudo-random and counterbalanced). Participants selected the ‘old’ photograph by pressing one of two keys (Z or X) on the keyboard. Participants were then prompted to report their confidence by clicking on a line that appeared below the images. Participants were told to click on the far-left side of the line if they were guessing, the far-right side of the line if they were absolutely confident that they were correct, and at points in between to reflect degrees of intermediate levels of confidence. These were coded on a scale from 0 (lowest rating) to 100 (highest rating). A green + or a red – appeared next to indicate their accuracy.

This procedure resulted in a 6×3 design, with *image type* (female face, male face, beach, forest, car, and chair) and *tone type* (no tone, distractor tone, and target tone) as within-participants factors. There were 32 trials per image type-by-tone condition for a total of 576 task trials over four runs. Trial order and spacing were optimized using the AFNI function `make_random_timing` to produce four sequences that minimized the amount of unexplained variance in a simulated task. Task trials were separated by 0–12 non-task trials.

Behavioral Data Analysis

To examine the effect of tone type on memory we fit a binomial generalized linear mixed effects model (Bates et al., 2015) to the recognition accuracy data with tone type as a fixed effect and with random intercepts for participant, old image, and new image [Accuracy \sim Tone + (1| Participant) + (1| Old) + (1| New)]. A linear mixed effects model was fit to participants’ recognition confidence ratings for correctly recognized images, with the same variables and random intercepts [Confidence \sim Tone + (1| Participant) + (1| Old) + (1| New)].

Tonic and Phasic Pupil Size Estimation and Analysis

Before estimating tonic and phasic pupil dilation on a trial-by-trial basis, pupil data for each participant and task run were preprocessed using the EyeLink DataViewer application (SR-Research, Canada), the FIRDeconvolution toolbox (Knappen et al., 2016), and custom routines. In brief, following the procedure outlined in Knappen et al. (2016), linear interpolation was used to estimate pupil size during blinks flagged by the EyeLink software and extended to include 100 ms margins before and after the blink. High-pass (0.1 Hz) and low-pass (10 Hz) Butterworth filters were applied, after which the data were down-sampled from 1,000 to 100 Hz. Noise associated with the end of blinks and saccades was then removed as follows. For each participant, mean pupil diameter was calculated for every sample during the

6 s time windows following a blink and following a saccade (pupil response). A double gamma impulse response function (IRF) was then fit to the pupil response following a blink. A single gamma IRF was fit to the pupil response following a saccade. The blink and saccade IRFs were convolved with blink and saccade ends to create individually tailored nuisance regressors, and a cleaned data set was then acquired by using the residuals from a linear model describing measured pupil responses as a function of these nuisance regressors. Finally, the previously filtered out slow drift was added back into the data, as this is a meaningful characteristic of pupil size over time.

Tonic pupil size and phasic pupil response were then estimated for each participant and trial of the encoding and detection task. For every trial, tonic pupil size was defined as the mean pupil size in the 500 ms window preceding the trial. In addition, phasic pupil responses were defined as the area under the curve (AUC, using Simpson's rule; Swallow et al., 2019), where the curve was the double gamma IRF that best fit the pupil time series during the 2 s interval following trial onset. Because AUC is the area between the phasic pupil's curve following trial onset relative to the pre-trial mean, trials with pupil dilation result in positive AUCs and trials with pupil contractions result in negative AUCs. AUC values were *z*-scored by subtracting the individual participant's mean AUC and dividing by the standard deviation to produce the *scaled phasic pupil response* (SPPR). A linear mixed effects model with random intercepts for image [SPPR ~ TonicPupilSize + (1| Old)] indicated a significant, negative relationship between the scaled phasic pupil responses and tonic pupil size, $\beta = -0.282$, 95% CI = [-0.320, -0.244], $t(2446) = -14.53$, $p < 0.001$. Due to scaling, random intercepts for participant had near-zero variance and were thus excluded from the model. Residuals from this model were used in subsequent analyses and are referred to as *phasic pupil responses* (PPR) for simplicity.

The effects of tone type on phasic pupil responses during encoding were evaluated by fitting a linear mixed effects model to the phasic pupil responses (averaged over presentations of an image) with tone type as a fixed effect and random intercepts for image [PPR ~ Tone + (1| Old)]. Random intercepts for participant had near-zero variance and were thus removed from the final model.

Univariate Analysis

Following pre-processing, EPI volumes with motion greater than 0.3 mm were excluded and the data were spatially smoothed using a Gaussian kernel until blur reached a full-width-half-maximum of 5.0 mm (3dBlurtoFWHM). To better estimate activity in the LC, voxels in the neighboring fourth ventricle, labeled with FreeSurfer (recon-all), were excluded from smoothing and subsequent analyses. In addition, masks defining the spatial extent of the brain in the aligned anatomical and EPI data sets, excluding the fourth ventricle, were applied to the EPI data. Data were scaled to a mean of 100 and a range of 0–200 to allow interpretation of beta weights as percent change.

Responses to events of different types were estimated for each voxel using 3dDeconvolve. All models included six motion regressors and 3rd order polynomial drift in baseline as nuisance variables. Regressors of interest were created by convolving a

delta function for each event of interest with the two-parameter SPMG2 hemodynamic response function (HRF; Henson et al., 2002). In the univariate encoding and detection task analyses, regressors were included for each combination of tone type and image type, for a total of 18 regressors of interest. When using the SPMG2 HRF, 3dDeconvolve produces two beta estimates for each condition. These were used to estimate the first 5 timepoints (12.5 s) of the hemodynamic response to each of the 18 conditions for subsequent group level analyses.

Univariate analyses of the ROIs were performed by extracting the mean estimated HRF across voxels located within the boundaries of the ROIs for each of the 18 conditions. For each ROI, estimated HRFs were additionally averaged across image type and analyzed in R with a linear mixed effects model that included tone type, time (timepoints 0 – 12.5 s), hemisphere (left and right), and all interactions as fixed effects and random intercepts for participant and image type [HRF ~ Time*Tone*Hem + (1| Participant) + (1| Image Type)]. The one exception was the LC ROI, which was collapsed across hemispheres [HRF ~ Time*Tone + (1| Participant) + (1| Image Type)]. Models were simplified by excluding the interactions with hemisphere for ROIs that did not show a hemisphere by tone type interaction [all but MC; HRF ~ Time*Tone + Hem + (1| Participant) + (1| Image Type)]. To characterize the effects of tone type over time in each ROI, general linear tests comparing activity across encoding conditions were then performed for each time point. Although all time points were tested, we focus on time points 2.5 – 7.5 s in our report. We expected the hemodynamic response to peak within that time frame because the stimuli were brief (cf. Hu et al., 2010) and the ABE, by its nature, should operate quickly.

Whole brain, group-level univariate analyses were performed to characterize the effects of target and distractor tones on activity throughout the brain. Voxels for which there was a significant interaction of tone type and time were identified in an analysis of variance with Type III sums of squares and tone type, image subcategory, and time (timepoints 0 – 12.5 s) as within participants factors, using 3dMVM (Chen et al., 2015). To further characterize the interaction of tone type and time, the statistical map for this interaction was thresholded at a False Discovery Rate of $q < 0.001$ (Genovese et al., 2002) to create a mask of voxels whose hemodynamic response significantly differed across the three tone type conditions. *Post hoc* paired *t*-tests (3dttest++) on voxels within the tone type by time interaction mask were performed on timepoints 2.5–7.5 s of the estimated HRF to target vs. distractor tones, target tones vs. no tones, and distractor tones vs. no tones. Statistical and cluster size thresholds were used to correct for multiple comparisons based on simulations that used spatial auto-correlation functions (using AFNI function 3dClustSim; Cox et al., 2017).

Trial-Specific Activity Estimation

Trial-specific activity was estimated by fitting a separate linear model for each trial of the encoding and detection task using the least square-separate approach (Mumford et al., 2012). The deconvolution was performed using AFNI's 3dDeconvolve with the SPMG2 option, such that each single-trial response was modeled by two regressors (a gamma response function and its

time derivative). Similarly, the combined responses on all other trials were modeled by two nuisance regressors. In addition, the design matrix included the same motion and drift nuisance variables used in the univariate model described above. The single-trial gamma function estimates were then saved, resulting in 576 (4 runs \times 144 trials) beta maps.

Beta Series Correlation Analysis

The effects of tone type on functional connectivity between the HPC and visual ROIs was estimated using beta series correlations (Rissman et al., 2004; Cisler et al., 2014; Geib et al., 2017) generated from the trial-specific activity estimates. To avoid introducing distortions, we did not subtract the mean pattern from each voxel or scale the data prior to computing these values (Garrido et al., 2013).

First, we concatenated the beta weights of trials sharing the same tone type condition (resulting in three series per voxel with 192 elements each). To obtain ROI-to-ROI functional connectivity estimates, separately for each tone type condition, we generated a mean beta series (obtained by averaging the series across voxels) for each ROI and computed pairwise Fisher-transformed Pearson correlations between those. We fit a linear mixed effects model to the correlation coefficients, with tone type and ROI pair as fixed factors and random intercepts for participant [Correlation \sim Tone*ROI + (1| Participant)]. Holm-corrected general linear tests comparing the different levels of tone type were performed.

ROI-to-voxel beta correlation analyses were then performed for each hippocampal ROI to test the hypothesis that communication should increase between the HPC and visual regions following target tones. Fisher-transformed Pearson correlations between the mean beta series of the seed ROI and each voxel in all visual and hippocampal ROIs (including those in the seed ROI) were then calculated for each tone type and participant. Linear mixed effects models (3dLME) with tone type as a fixed effect and random intercepts for participant were then fit to the ROI-to-voxel correlations [Correlation \sim Tone + (1| Participant)]. General linear tests contrasted the target with the distractor and no tone conditions at each voxel. Candidate clusters in the resulting maps were identified after accounting for spatial autocorrelation in the data (estimated with 3dFWHMx) and by thresholding based on a minimal cluster size and maximal p -value (voxel edges must touch, $\alpha = 0.05$, uncorrected $p = 0.05$; 3dClustSim and 3dClusterize; Cox et al., 2017). This was followed by confirmatory analyses in which each cluster was treated as an ROI. The correlation between the average beta series of the ROI and that of the respective hippocampal seed was computed separately for each participant. A linear mixed effects model, with tone type as a fixed effect and random intercepts for participant, was fit to the correlations [Correlation \sim Tone + (1| Participant)]. Follow-up general linear tests contrasting the tone type conditions were then performed. This was done to ensure that the clustering procedure did not produce spurious clusters.

Support Vector Classification

On their own, differences in BOLD magnitude do not necessarily indicate changes in the quality or extent of stimulus processing

(e.g., Ward et al., 2013; Hatfield et al., 2016). We therefore used linear support vector machine (SVM) classification (Suykens and Vandewalle, 1999; Hsu and Lin, 2002) to probe the effects of target tone detection on image category decoding accuracy in the visual and hippocampal ROIs (V1, V2, FG, PG, aHPC, and pHPC). The algorithm estimates a hyperplane that maximizes the margin between it and samples that belong to different classes (Suykens and Vandewalle, 1999; Hsu and Lin, 2002). It is among the most common approaches to multivoxel pattern analysis (Mahmoudi et al., 2012; Haxby et al., 2014; Diedrichsen and Kriegeskorte, 2017). Importantly, it sidesteps many of the interpretability issues inherent to representational similarity analysis (cf. Walther et al., 2016).

Each trial-wise beta map was assigned one of six labels indicating the type of image presented on that trial. Individual beta series maps were standardized across trials such that each voxel had a mean of zero and a standard deviation of one. Classification accuracy was estimated for each tone type and ROI using repeated fourfold cross validation. Balanced training sets of 144 trial-wise beta maps were randomly drawn 30 times (the remaining 48 trials in each iteration were reserved as a test set); on each iteration a new linear SVM ($C = 1$, one-vs.-one multiclass, default implementation in scikit-learn 0.21.2; Pedregosa et al., 2011) was fit to the training set and applied to the test set to obtain a confusion matrix and a classification accuracy estimate for each tone type condition. These were averaged across the 30 iterations to produce one estimate and one confusion matrix for each combination of participant, tone type, and ROI. The effects of tone type on mean classification accuracy were evaluated for each ROI using a linear mixed effects model with tone type as a fixed effect and random intercepts for participant [Accuracy \sim Tone + (1| Participant)].

Locus Coeruleus Functional Connectivity

ROIs that exhibited functional connectivity with LC during rest were identified using resting state data reported in Turker et al. (2021). Briefly, intrinsic functional connectivity (iFC) maps were created for each participant using denoised multi-echo data and the participant's individually defined LC ROI. Data were denoised using ME-ICA (Kundu et al., 2013), bandpass filtered ($0.01 < f < 0.1$), and were not additionally blurred. A group-level iFC map was created using voxel-wise t -tests (3dttest++) and a one-sided clustering procedure at $p = 0.01$ and FDR = 0.018 [3dClusterize; corrected for multiple comparisons using the false discovery rate (FDR = 0.02; Genovese et al., 2002)]. Twenty ranked peaks were extracted from the group iFC map (3dmaxima) with a minimal distance of 18 mm (6 voxels) between peaks. Next, 6 mm spherical ROIs were constructed around those peaks and a final set of 20 ROIs was obtained by intersecting the spheres with the group-level iFC map thresholded at $p < 0.001$, $q < 0.004$, producing the final LC-iFC ROIs (**Supplementary Table 1**).⁴

⁴Though the regions are similar, the exact coordinates and rank order of ROIs in **Supplementary Table 1** differ from those reported in Turker et al. (2021) because of a difference in coordinate systems and a change in how data were compressed during preprocessing.

Statistical Software

All group-level analyses were performed in R v3.6.1 (R Core Team, 2013) or in AFNI v16.2.07 (using 3dLME or 3dMVM). Unless otherwise noted, linear mixed effects models were fit using lme4 v1.1.21 (Bates et al., 2015). Type III (Satterthwaite's method) ANOVA tables were obtained using the 'joint_tests' function in the package emmeans v1.3.5.1 (Length, 2020). General linear tests were performed and uncorrected confidence intervals were obtained using the emmeans functions 'contrasts' and 'confint.' In all analyses, Holm-Bonferroni adjusted p -values were computed separately for each set of tone type comparisons. Confidence intervals, where reported, are uncorrected.

RESULTS

Behavioral Task Performance and Whole Brain Analysis

Participants accurately performed the detection task, pressing the button for $M = 97.5\%$ of the targets, $SD = 0.15$, 95% CI = [0.970, 0.990], $M = 5.1\%$ of the distractors, $SD = 0.22$, 95% CI = [0.023, 0.060] and $M = 0.2\%$ of the no tone trials, $SD = 0.05$, 95% CI = [0.001, 0.003]. Incorrect button presses were more likely to follow a distractor tone than no tone, $t(20) = -4.16$, $p < 0.001$, $d = 1.25$.

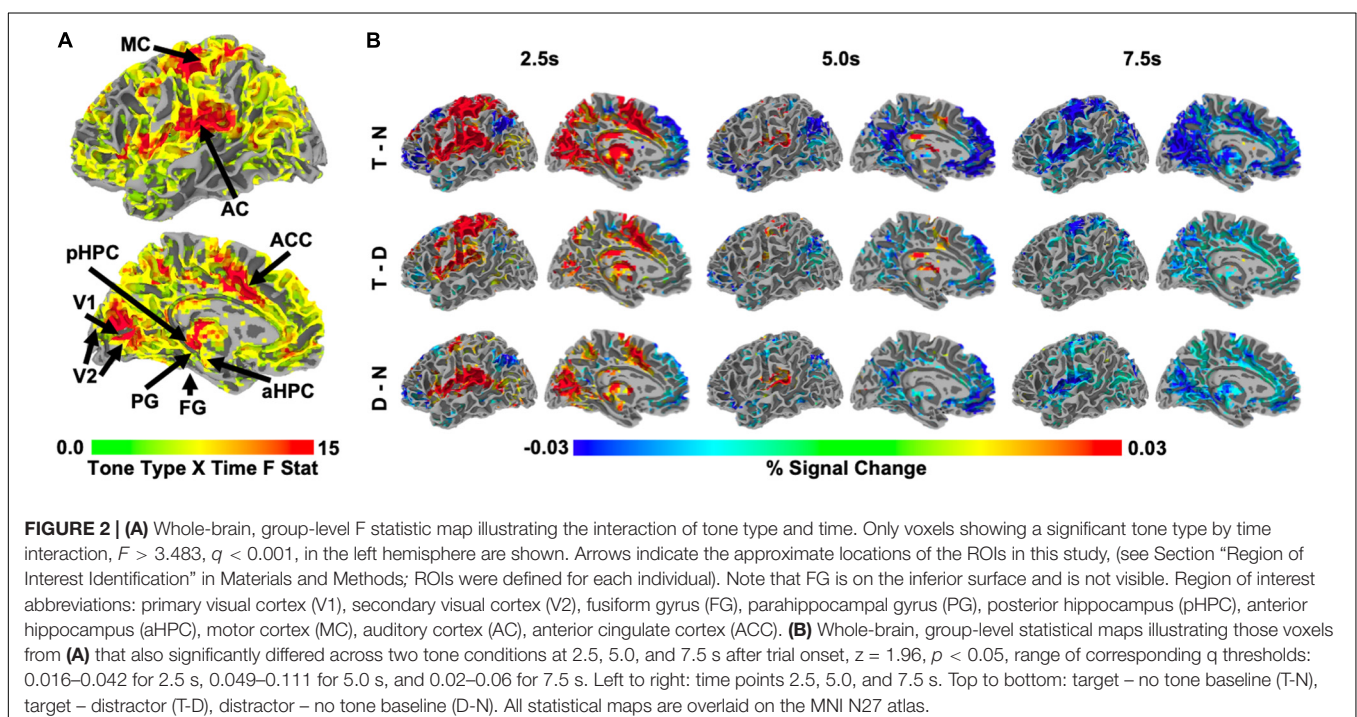
The tone type condition did not significantly influence image recognition accuracy, $F(2, \text{inf}) = 1.08$, $p = 0.34$. However, it did influence the confidence with which images were correctly recognized, $F(2, 1660.8) = 6.81$, $p = 0.001$. Participants reported higher levels of confidence for correctly recognized images paired with a target than for those paired with a distractor ($M_{Diff} = 5.58$),

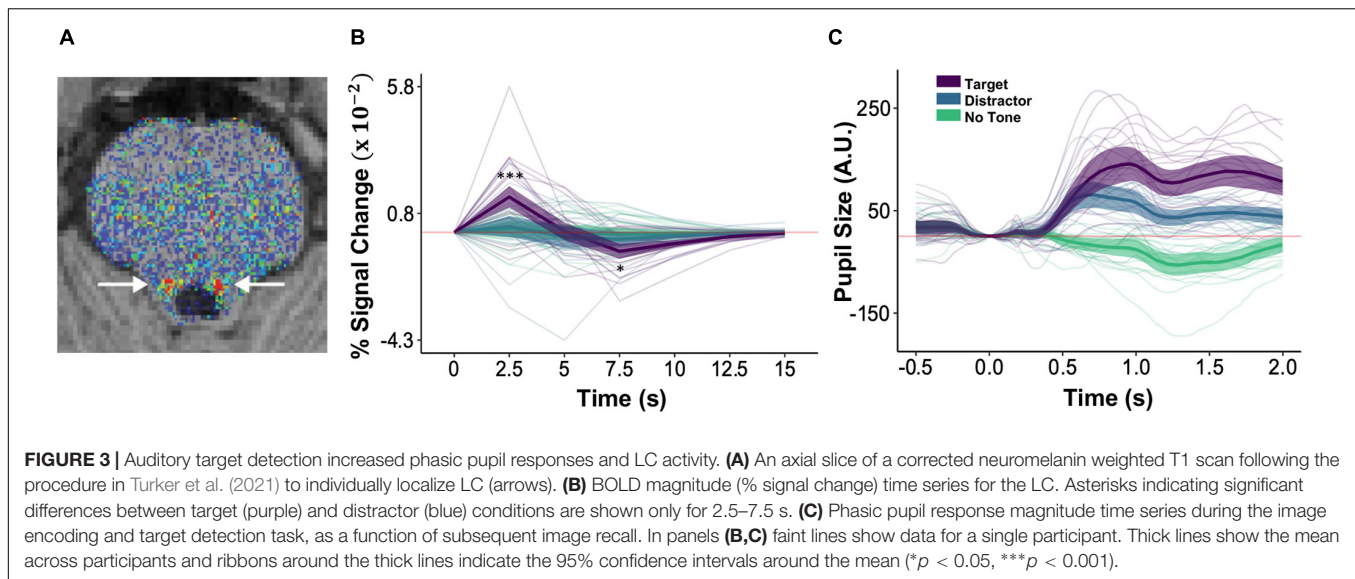
95% CI = [1.83, 9.32], $t(1899.08) = 3.57$, $p = 0.001$, $d = 0.57$, or presented without a tone ($M_{Diff} = 4.10$), 95% CI = [0.23, 7.97], $t(1573.68) = 2.54$, $p = 0.023$, $d = 0.44$, but confidence did not differ between correctly recognized images presented in the distractor and no tone conditions ($M_{Diff} = 1.48$), 95% CI = [-2.38, 5.34], $t(1578.25) = 0.92$, $p = 0.359$, $d = 0.10$. Target detection during image encoding thus increased the confidence with which those images were later correctly recognized, and distractor rejection did not significantly interfere with the encoding of a concurrently presented image (Figure 1B).

Whole brain analyses revealed that auditory target detection influenced BOLD activity in regions spanning medial occipital, medial parietal, anterior cingulate, superior temporal, middle frontal, and subcortical areas, including thalamus (time by tone type interaction, $F > 3.483$, $q < 0.001$; Figure 2A). In many of these regions, activity was initially higher on the target tone trials than in the other two types of trials, though this relationship reversed at subsequent timepoints (Figure 2B, top and middle row). Relative to no tone trials, the response to distractor trials was smaller in magnitude than the response to target trials in most regions (Figure 2B, bottom row).

Locus Coeruleus and Phasic Pupil Responses

To test our hypothesis that the LC is involved in the ABE, we examined whether target tone trials evoked greater phasic pupil responses and LC signal changes than did distractor tone and no tone trials. Consistent with this possibility, BOLD responses in the hand-traced LC ROIs (Figure 3A) exhibited an interaction of tone type and time, $F(10, 2225) = 8.28$, $p < 0.001$, reflecting greater increases in activity at 2.5 s on target tone trials than on





distractor tone trials, $t(2225) = 6.51$, $p < 0.001$, $d = 0.48$, and no tone trials, $t(2225) = 7.03$, $p < 0.001$, $d = 0.58$ (**Figure 3B**). Phasic pupil responses also varied across tone type, $F(2,2124.6) = 336.98$, $p < 0.001$: they were more positive on trials that included a target tone than on trials that included a distractor tone ($M_{Diff} = 0.47$), 95% CI = [0.37, 0.56], $t(2110) = 11.45$, $p < 0.001$, $d = 0.25$, or no tone ($M_{Diff} = 1.05$), 95% CI = [0.96, 1.15], $t(2102) = 25.86$, $p < 0.001$, $d = 0.39$. They were also greater on distractor tone trials than on no tone trials ($M_{Diff} = 0.59$), 95% CI = [0.49, 0.68], $t(2160) = 14.44$, $p < 0.001$, $d = 0.13$ (**Figure 3C**). These data demonstrate increased activity of the LC system on trials that require a response and provide no evidence for inhibitory effects of distractor rejection on this system.

BOLD Responses in Perceptual and Motor Regions

To examine the effects of target detection on the processing of episodic information, planned analyses tested whether tone type modulated BOLD magnitude within regions involved in stimulus processing, encoding, and response generation: bilateral MC, V1, V2, FG, PG, aHPC, and pHPC. These analyses evaluate whether previously reported effects of auditory target detection on BOLD responses in visual cortex (Swallow et al., 2012) (1) reflect an increase over a neutral baseline condition as well as over distractor conditions, and (2) are present in other regions important for episodic encoding.

The interaction of tone type and time was significant in V1, V2, FG, PG, aHPC, and pHPC, smallest $F(10,4492) = 12.48$, $p = 0.001$ for FG. Extending earlier reports (Swallow et al., 2012), V1 showed a larger initial increase in activity on target trials than on both distractor and no tone trials, smallest $z = 7.81$, $p < 0.001$, $d = 0.43$. Similar increases were also observed in V2, FG, and PG, smallest $z = 2.60$, $p = 0.019$, $d = 0.15$, as well, demonstrating that these effects can also be detected in higher-level visual regions as well as in early visual cortex. Additionally, in all cases BOLD activity showed a steeper drop-off in magnitude on target trials

relative to distractor and no tone trials (**Figure 4** and see also **Supplementary Figure 1**).

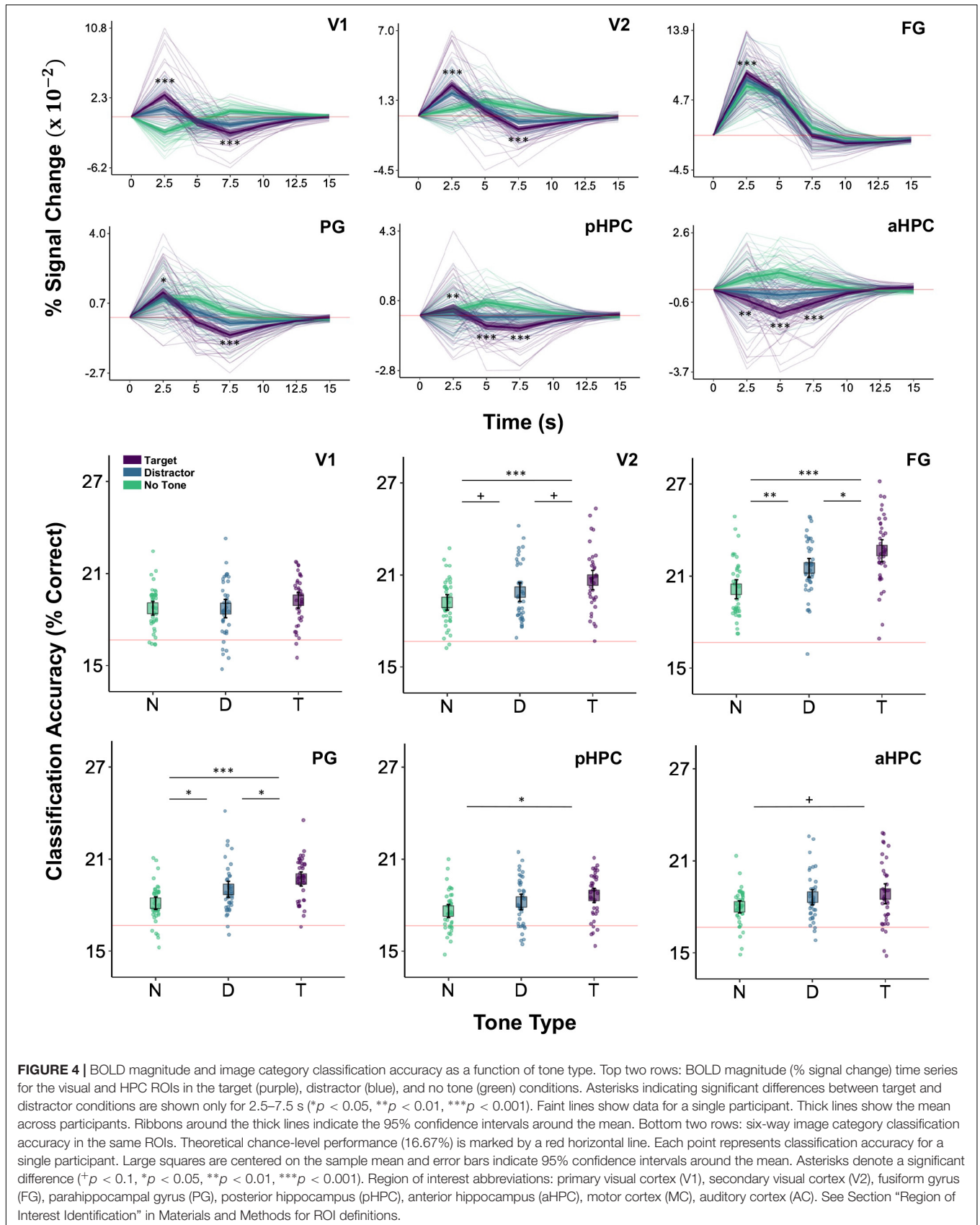
The HPC generally showed larger decreases in activity on target trials than on distractor and no tone trials. This was true of both the aHPC and pHPC, which at 5 s were more strongly deactivated on target trials than on distractor trials, smallest $z = 4.50$, $p = 0.001$, $d = 0.28$, and no tone trials, smallest $z = 11.81$, $p < 0.001$, $d = 0.751$. However, activity in the aHPC decreased more rapidly than it did in the pHPC: at 2.5 s, activity in the aHPC was lower on target than on distractor, $z = 3.12$, $p = 0.002$, $d = 0.18$, and no tone, $z = 8.54$, $p < 0.001$, $d = 0.52$, trials, whereas activity in pHPC was higher on target trials than on distractor trials, $z = 3.49$, $p = 0.001$, $d = 0.20$ (**Figure 4**).

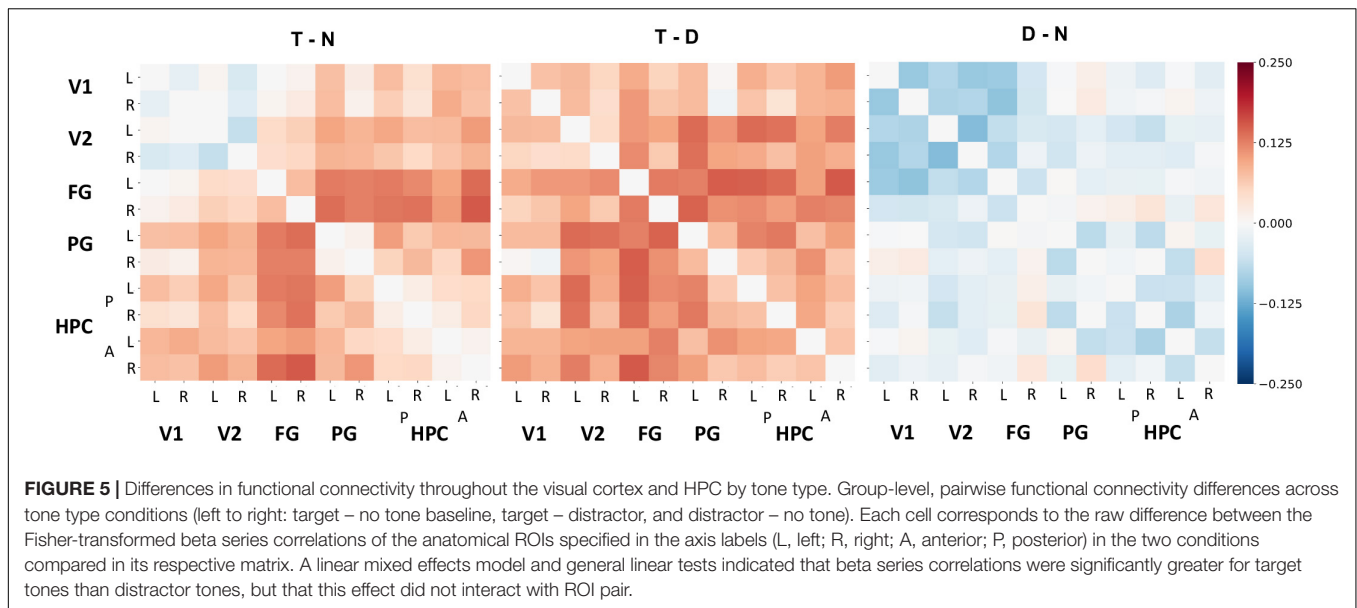
Except for in the MC, there were no interactions between hemisphere and tone type, largest $F(2,4475) = 1.80$, $p = 0.165$, or between tone type, time, and hemisphere, largest $F(10,4475) = 1.77$, $p = 0.061$. In MC, at 2.5 s, BOLD activity was greater on target trials than on distractor and no tone trials in the left hemisphere, smallest $t(2225) = 13.55$, $p < 0.001$, $d = 0.98$.

These results demonstrate that target detection modulated the magnitude of activity in regions involved in representing visual and episodic information.

Decodable Stimulus Information in the Visual Cortex and Hippocampus

Increased BOLD activity on target trials does not necessarily entail that processing in these regions is enhanced. To test our hypothesis that target detection facilitates the processing of concurrently presented images, we conducted analyses of image category classification accuracy using voxel-wise patterns of activity in the visual and hippocampal ROIs. These revealed a main effect of tone type in V2, FG, PG, and pHPC, smallest $F(2,92) = 4.59$, $p = 0.013$ for pHPC, but not in V1 or aHPC, largest $F(2,92) = 1.36$, $p = 0.261$ for V1. Follow up analyses indicated that classification accuracy was higher on target trials than on no tone trials in V2, FG, PG, and pHPC, smallest





$t(92) = 3.01, p = 0.01, d = 0.96$ for pHPC. Classification accuracy was also higher on target compared to distractor tone trials in FG $t(92) = 2.60, p = 0.011, d = 0.62$, PG, $t(92) = 2.09, p = 0.039, d = 0.52$, and marginally in V2, $t(92) = 2.17, p = 0.065, d = 0.44$. Similarly, relative to no tone trials, distractor trials significantly enhanced classification accuracy in FG and PG, smallest $t(92) = 2.764, p = 0.014, d = 0.87$ for the latter, and showed a marginal effect in V2, $t(92) = 1.88, p = 0.065, d = 0.43$ (Figure 4). Thus, regions whose activity was enhanced by target detection also exhibited within-ROI patterns of activity that better correlated with image category on these trials than on distractor or no tone trials. This was particularly true in higher-level visual areas, FG and PG, which should be more tuned to image categories than V1 and V2.

Visuo-Hippocampal Functional Connectivity

To test our hypothesis that target detection enhances communication between regions involved in episodic processing, functional connectivity between all visual and hippocampal ROIs was quantified with beta series correlations (Figure 5). Our analysis examined the effect of tone type across each pairing of the following ROIs: l/r-V1, l/r-V2, l/r-FG, l/r-PG, l/r-aHPC, and l/r-pHPC. Tone type and ROI pair influenced functional connectivity, $F(2, \text{inf}) = 46.65, p < 0.001$ and $F(77, \text{inf}) = 122.24, p < 0.001$, respectively, but did not interact, $F(154, \text{inf}) = 0.33, p > 0.999$. Holm-corrected general linear tests indicated that functional connectivity was enhanced on target trials relative to both distractor trials, $z = 9.48, p < 0.001, d = 0.50$, and no tone trials, $z = 6.36, p < 0.001, d = 0.32$. Functional connectivity was also higher on no tone trials than on distractor tone trials, $z = 3.12, p = 0.002, d = 0.24$. Thus, relative to the no tone trials, target tones increased correlations between ROIs while distractor tones decreased them.

To more precisely identify the regions whose functional connectivity with the HPC changed with tone type, we calculated ROI-to-voxel functional connectivity maps and extracted candidate clusters by contrasting the tone type conditions. We refer to these clusters by the ROI seed that generated them and the anatomical area that they overlapped with most (e.g., l-pHPC < - > r-V2 refers to a cluster largely overlapping with r-V2 that was correlated with l-pHPC). No clusters were found when the distractor condition was contrasted with the no tone baseline, indicating that the distractor tones did not reliably alter functional connectivity between the HPC and visual cortex. However, three clusters (l-pHPC < - > l-FG, l-pHPC < - > r-FG, and r-aHPC < - > l-FG) were identified when target trials were contrasted with no tone trials and seven clusters were identified when target trials were contrasted with distractor trials (Table 1 and Figure 6). Both sets of clusters spanned voxels throughout visual cortex.

Confirmatory analyses on clusters identified in the target versus distractor contrast were performed by averaging functional connectivity across all voxels within a cluster and then testing the effect of tone type in a linear mixed effects model. This analysis indicated that all pairs showed an effect of tone type on functional connectivity, smallest $F(2,36) = 3.77, p = 0.033$ for l-aHPC < - > r-FG, except l-aHPC < - > l-FG, $F(2,36) = 3.02, p = 0.061$. In those pairs showing an effect of tone type, functional connectivity was higher on target trials than on distractor trials, smallest $t(36) = 2.61, p = 0.039, d = 0.54$ for l-aHPC < - > r-FG. Functional connectivity was also higher on target trials than on no tone trials in the pairs l-pHPC < - > r-V2, l-pHPC < - > l-V2, and r-aHPC < - > l-FG, smallest $t(36) = 2.39, p = 0.045, d = 0.46$ for l-pHPC < - > l-V2. No differences in functional connectivity were found between the distractor and no tone trials in any of the clusters, largest $t(36) = 1.12, p = 0.273, d = 0.29$ (Figure 6).

To test the hypothesis that increased visuo-hippocampal coordination during target tone trials is associated with better

TABLE 1 | Clusters showing higher functional connectivity with the HPC on target tone than on distractor tone trials in the seed-to-voxel beta series correlation analysis.

Seed	Cluster	Center of Mass	Size	% overlap with anatomical ROIs							
				l-V1	r-V1	l-V2	r-V2	l-FG	r-FG	l-PG	r-PG
l-pHPC	r-V2	-16.0, 72.5, -1.1	264	0.8%	23.6%	1%	50.2%	-	24.4%	-	-
l-pHPC	l-V2	20.3, 69.0, -10.8	253	8.3%	-	48.8%	-	42.9%	-	-	-
l-aHPC	l-FG	32.4, 52.6, -17.9	60	-	-	-	-	100%	-	-	-
l-aHPC	r-FG	-30.5, 61.9, -13.9	43	-	-	-	10.5%	-	89.5%	-	-
r-pHPC	l-V2	10.8, 74.1, -5.4	102	17.5%	-	79%	-	3.5%	-	-	-
r-pHPC	r-FG	-22.9, 64.3, -10.7	56	-	1.2%	-	48.9%	-	49.9%	-	-
r-aHPC	l-FG	25.1, 66.4, -14.5	148	1%	-	37.5%	-	61.5%	-	-	-

Center of mass is reported in Right Anterior Inferior coordinates (RAI, the AFNI default), volumes are in mm^3 , and the percentages of voxels in a cluster that overlapped with each anatomical ROI are the mean across subjects.

visual processing, we treated the ROI-to-voxel functional connectivity clusters as ROIs in an image category classification analysis. Tone type affected classification accuracy in all clusters except r-pHPC $\langle - \rangle$ l-V2, smallest $F(2,36) = 3.53$, $p = 0.04$. This effect reflected greater accuracy on target trials than on no tone trials, smallest $t(36) = 2.65$, $p = 0.035$, $d = 0.86$. Only the l-pHPC $\langle - \rangle$ r-V2 cluster showed higher classification accuracy on target trials than on distractor trials, $t(36) = 2.54$, $p = 0.031$, $d = 0.74$. Accuracy was higher on distractor trials than on no tone trials in r-pHPC $\langle - \rangle$ r-FG and r-aHPC $\langle - \rangle$ l-FG, smallest $t(36) = 2.48$, $p = 0.036$, $d = 0.77$ for the former (Figure 6).

Functional Connectivity of Regions Associated With the Locus Coeruleus

A functional connectivity analysis with the LC as a seed revealed small regions within l-FG, r-FG, and r-HPC that showed higher functional connectivity with the LC in the target tone condition than in the distractor tone condition (respectively, $ps > 0.007$, $ps > 0.012$, $ps > 0.045$; illustrated in Supplementary Figure 4). However, these regions were not large enough to survive corrections for multiple comparison using cluster size 32 ($\alpha < 0.05$). Voxels in l-MC also showed no evidence of differential connectivity with the LC on target relative to distractor trials, suggesting that this analysis may not have been powerful enough to detect differences in LC connectivity across conditions.

However, if the LC influences activity in regions involved in episodic encoding, then functional connectivity between HPC and regions whose activity is modulated by the LC during rest should be greater on target trials (when LC activity is strongest) than on distractor and no tone trials. To test this hypothesis, a set of 20 regions whose activity was associated with LC activity during a separate resting state scan—referred to as LC-iFC ROIs—were identified (see Section “Region of Interest Identification” in Materials and Methods and Turker et al., 2021; Supplementary Table 1) and their functional connectivity to the four hippocampal seeds was examined. A separate model was fit for each of l-pHPC, r-pHPC, l-aHPC, and r-aHPC.

Main effects were found for tone type, smallest $F(2,1062) = 10.11$, $p < 0.001$ for l-aHPC, and region, smallest $F(19,1062) = 13.05$, $p < 0.001$ for r-pHPC, but the two did not interact, largest $F(38,1062) = 0.49$, $p = 0.996$ for l-pHPC. General linear tests that collapsed across LC-iFC ROIs showed higher functional connectivity on target trials than on distractor

trials, smallest $t(1062) = 4.45$, $p < 0.001$, $d = 0.41$ for l-aHPC, and no tone trials, smallest $t(1062) = 2.45$, $p = 0.029$, $d = 0.24$ for l-pHPC. Functional connectivity to l-pHPC was lower on distractor trials than on no tone trials, $t(1062) = 2.06$, $p = 0.039$, $d = 0.32$. Tone type did not significantly influence functional connectivity between the LC and the LC-iFC ROIs, $F(2,1062) = 0.093$, $p = 0.911$, consistent with the possibility that functional connectivity analyses of LC during the encoding task were not sufficiently powerful.

DISCUSSION

In this fMRI study, we investigated the effects of target detection on how visual stimuli are processed and encoded by the brain. We examined how visual regions, the HPC, and the LC respond to images presented concurrently with an auditory target tone (requiring a motor response), a distractor tone (requiring no response), or no tone. The inclusion of a no tone baseline condition, which was absent in previous fMRI studies of similar effects, allowed us to test for both target-induced enhancement and distractor-induced disruption of encoding, perceptual processing, and functional connectivity. We found that, relative to both other conditions, target tones enhanced image recognition confidence (the ABE), the magnitude of phasic pupil responses, activity in LC and in visual regions, visuo-hippocampal functional connectivity, and image category classification accuracy from multivoxel patterns in FG and PG. Combined, these results suggest that auditory target detection enhances the processing of visual information by increasing inter-areal communication and enhancing the specificity of visual representations.

Consistent with existing evidence suggesting that target detection enhances episodic encoding in the attentional boost effect (Swallow and Jiang, 2013), recognition confidence ratings for correctly remembered images were greater when those were paired with a target tone as opposed to a distractor tone. Indeed, previous work has shown that target detection can enhance both recollection and familiarity of images presented during the encoding task even when they are presented one time (Broitman and Swallow, 2020). The absence of significant differences in recognition accuracy in the full sample is consistent with an earlier MRI study (Swallow et al., 2012) and may be a

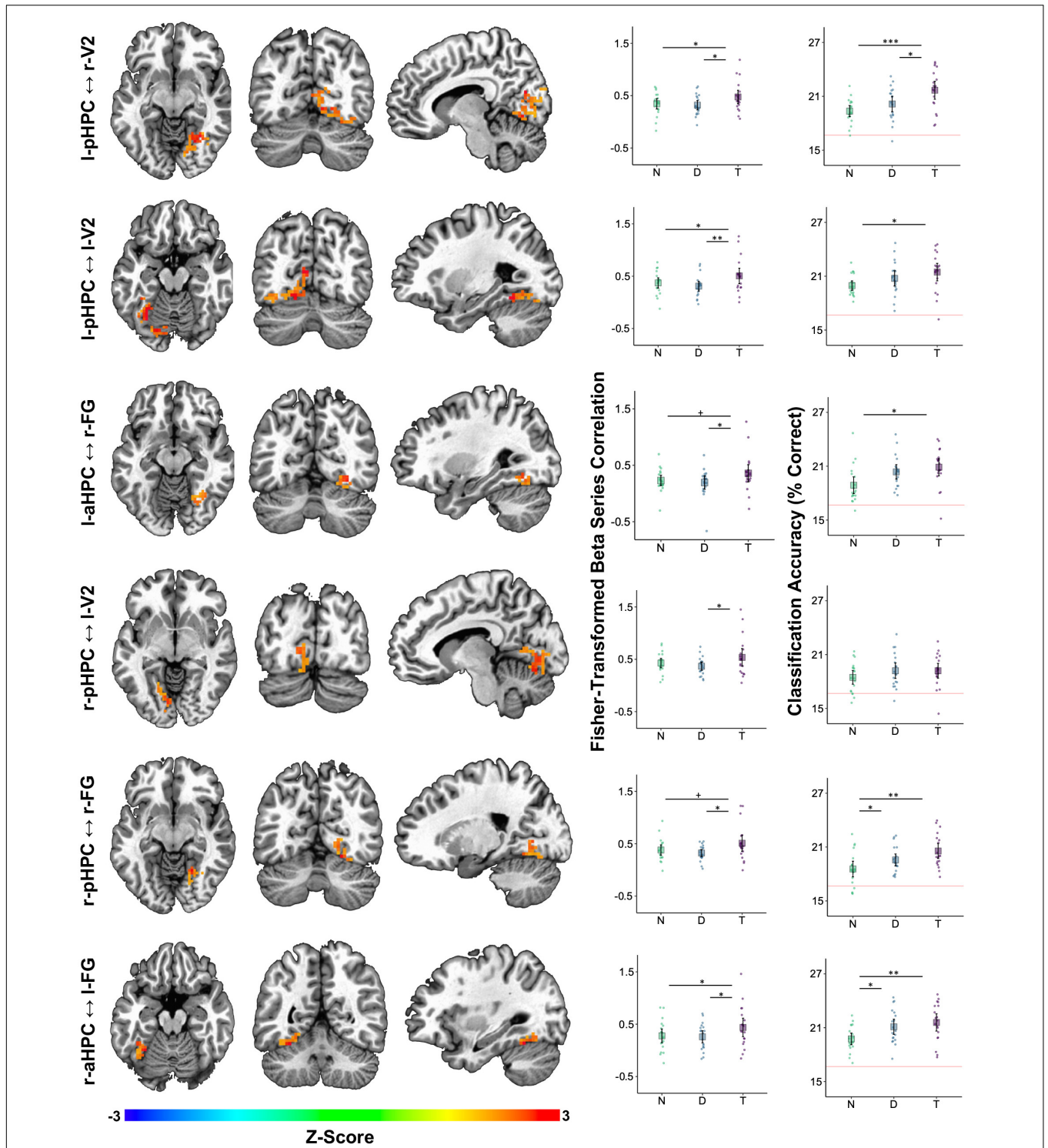


FIGURE 6 | Auditory target detection improved image classification accuracy in visual regions showing increased functional connectivity with the HPC. Each row corresponds to one cluster detected as being more strongly correlated with the HPC on target tone trials than on distractor tone trials. The seed-cluster pair label is denoted on the left. Left three columns: voxel colors correspond to z-scores obtained by contrasting the Fisher-transformed correlations between the mean beta series for the hippocampal seed region and that of each voxel in V1, V2, FG, PG, pHPC, and aHPC. Middle column: mean Fisher-transformed beta series correlations between each cluster and its respective hippocampal seed, obtained separately for each tone type condition—no tone (N), distractor tone (D), and target tone (T). Right column: six-way image category classification accuracy for each cluster. Theoretical chance-level performance (16.67%) is marked by a red horizontal line. Middle and Right columns: large squares are centered on the sample mean and error bars indicate 95% confidence intervals around the mean. Each point represents an observation from a single participant. Asterisks denote a significant difference ($^+p < 0.1$, $*p < 0.05$, $**p < 0.01$, $***p < 0.001$).

consequence of the relatively long inter-trial intervals that had to be used in this study (cf. Mulligan and Spataro, 2015).

Throughout the visual areas examined, activity in the target tone condition was higher relative to the distractor and no-tone baseline conditions. This pattern was also present in other regions involved in orienting to relevant stimuli. Those included the thalamus, whose higher-order nuclei play a critical role in attention and in the maintenance of sensory representations in awareness and working memory (Saalmann and Kastner, 2011), and the LC, whose noradrenergic projections regulate gain throughout the cortex (Servan-Schreiber et al., 1990; Aston-Jones and Cohen, 2005) and which tends to exhibit larger responses following salient events (Bouret and Sara, 2005). Interestingly, the opposite pattern was observed in aHPC and pHPC: activity decreased on target tone trials relative to the two other conditions. Because the images were presented four times, these decreases may reflect greater repetition suppression of hippocampal activity for target-paired images than for other images (Henson and Rugg, 2003; Summerfield et al., 2008; Larsson and Smith, 2012; Kim et al., 2020). Measures of repetition suppression tend to positively correlate with subsequent recognition memory (e.g., Pihlajamäki et al., 2011) and with functional connectivity between the HPC, visual cortex, and prefrontal cortex (Zweynert et al., 2011). Though our results, as a whole, hint at a relationship between hippocampal repetition suppression and the effects of target detection on recollection, additional work is needed to confirm this possibility.

Changes in inter-areal coordination are thought to play a role in the maintenance and encoding of neural representations (Fries, 2005, 2015; Singer, 2013; Bonnefond et al., 2017; Moyal and Edelman, 2019; Moyal et al., 2020). Enhanced cortico-hippocampal functional connectivity, in particular, has been associated with working memory maintenance and long-term memory encoding (e.g., Gazzaley et al., 2004; for a review, see Poch and Campo, 2012). Target detection could influence perception and memory in a similar fashion, by enhancing communication between perceptual and medial temporal regions in critical moments (e.g., when responding to targets). Our findings are compatible with this idea: functional connectivity between aHPC and pHPC and the visual cortex was higher on target tone trials relative to both distractor and no tone trials. The effect of target tones on HPC to visual cortex functional connectivity was most pronounced for the left pHPC, which showed widespread, bilateral increases in functional connectivity with clusters in the ventral visual cortex—V1, V2, and FG. The aHPC exhibited a similar correlation with FG, but less so with V1 and V2. Differences in the effects of target detection on aHPC and pHPC connectivity are consistent with the differential functional connectivity of the anterior and posterior HPC previously reported in humans (Poppenk et al., 2013; Frank et al., 2019). They also suggest that future research should examine whether target detection has larger effects on the types of information processed by pHPC (perceptual features of stimuli) than on the types of information supported by aHPC (categories of stimuli).

The target-related enhancement of visuo-hippocampal connectivity was accompanied by a boost in image category classification accuracy throughout the ventral visual stream and in pHPC relative to the baseline condition. A similar

enhancement was found relative to the distractor tone condition in FG and PG. This suggests that the effect of target detection on subsequent recognition confidence could reflect improved perceptual encoding in higher level visual areas. Surprisingly, a smaller increase in classification accuracy was also observed on distractor tone trials relative to the no-tone baseline in FG and PG. Thus, although exposure to any auditory tone in this task may enhance the quality of visual information processing, target detection provides an additional boost. A similar pattern was also found in smaller ventral visual clusters that exhibited greater functional connectivity with HPC on target compared to distractor tone trials. This suggests a possible relationship between these two effects. Future studies may address the question of whether shifts in long-range coordination are directly related to the quality and extent of perceptual processing and memory encoding (Moyal and Edelman, 2019)—not only in terms of multivoxel classification accuracy and recognition confidence (as demonstrated in this study), but also in terms of subsequent memory test performance.

Phasic LC responses have been hypothesized to facilitate the updating of representations and contribute to the ABE (Swallow and Jiang, 2010; Swallow et al., 2012) by enhancing perceptual processing following target detection independent of modality or spatial location (Nieuwenhuis et al., 2005; Swallow and Jiang, 2013, 2014; see also Bouret and Sara, 2005). Our results are consistent with this view. They suggest a role for the LC in mediating the effects of target detection on perception and memory via the strengthening or reorganization of functional networks. In this study, both LC activity and phasic pupil responses (which may correlate; Joshi et al., 2016) increased on target tone trials relative to both distractor and no tone trials. These differences were observed despite the fact that each condition was equally likely. However, whereas LC activity did not increase on distractor trials relative to no tone trials, pupil diameter did. Indeed, other cognitive and neural factors contribute to pupil size in addition to LC activity (e.g., cognitive effort; van der Wel and van Steenbergen, 2018). Additionally, regions that were highly correlated with the LC during rest were also more strongly correlated with aHPC and pHPC on target trials than on distractor trials during the encoding task. Though a contrast of functional connectivity between LC and our cortical and hippocampal ROIs only yielded a marginal increase on target tone trials (reported in the **Supplementary Materials**), these findings hint at a possible link between target-related LC responses and the other effects we observed, which can be addressed directly in future studies.

In the encoding and detection task, target detection differs from distractor rejection in both cognitive and motor demands. However, the effects of target detection on activity in visual cortex, pupil responses, and memory can occur in the absence of an overt motor response and are absent when motor responses are self-generated (Jack et al., 2006; Swallow and Jiang, 2012; Swallow et al., 2012, 2019; Makovski et al., 2013; Mulligan et al., 2016; Toh and Lee, 2022). In this study, behavioral inhibition in the distractor tone condition also did not lower BOLD magnitude or classification accuracy relative to the baseline, arguing against the possibility of a disruptive effect of response inhibition on processing (as in inhibition-induced forgetting, which has been

tied to fluctuations in ventrolateral PFC activity, which were not found here; Chiu and Egner, 2015). While this confirms that our findings reflect a target-induced boost (Swallow and Jiang, 2014), target detection was confounded with motor responses in this study. Therefore, additional research is necessary to identify and confirm the source of the physiological effects we report here, whether it is from the motor system or otherwise (see **Supplementary Materials** for additional analyses).

Though the peak BOLD responses we observed were often earlier than is typical in human fMRI, they are consistent with expected BOLD response latencies (Miezin et al., 2000) and fall within the range of peak latencies reported in investigations of hemodynamic response variability (Handwerker et al., 2004) and BOLD responses to brief (<1 s) auditory tones (Hu et al., 2010). Rapid BOLD dynamics in our study may also reflect the relatively coarse temporal resolution of the EPI sequence (TR = 2.5 s), as well as the duration and periodicity of stimulus presentation in our task: BOLD responses are sharper and faster when stimuli are brief (Huettel et al., 2004; Tian et al., 2010; Hirano et al., 2011) and both effects may be exaggerated when brief stimuli are presented over a background of periodic stimulation (Lewis et al., 2016). Animal neuroimaging and physiological modeling further suggest that rapid increases and decreases in BOLD signal reflect changes in blood flow and volume within microvasculature supporting temporally and spatially localized neuronal activity (Tian et al., 2010; Hirano et al., 2011; Polimeni and Lewis, 2021). The rapid BOLD dynamics we observed therefore may reflect temporally and spatially precise neural responses to brief stimuli presented during periodic visual change.

Taken together, our data provide novel evidence that target detection facilitates the processing and encoding of information presented at the same time as stimuli that require a response. These events enhance perceptual processing and functional connectivity between the HPC and the ventral visual cortex. Both effects could be related to the stronger LC responses observed following auditory target detection. Our results and interpretation are compatible with the emerging view that, by increasing gain throughout the thalamocortical network at opportune moments, the phasic release of NE from the LC may facilitate functional network reorganization and promote more integrated, information-rich dynamics. Theoretical models and empirical findings have linked higher gain to increases in the topological complexity and variability of population activity (Shine et al., 2018; Moyal and Edelman, 2019) as well as to enhanced inter-regional information transfer (Li et al., 2019). Though LC-mediated changes in gain may be sufficient for mediating the facilitatory effects of target detection on memory, prefrontal influences are also likely to contribute—either by modulating LC output (Jodoj et al., 1998) or by directly regulating hippocampal activity and functional connectivity to support memory encoding (Ranganath et al., 2005; Schott et al., 2013). Future work may combine functional neuroimaging, electrophysiology, and computer simulations to explore these possibilities and provide a precise account of the mechanisms underlying the ABE. This work can further clarify the effects of attending to behaviorally relevant moments on neural dynamics, information representation, and incidental encoding.

DATA AVAILABILITY STATEMENT

The datasets presented in this article are not readily available because participants did not provide consent to make their data publicly available. Data are available from the corresponding author upon reasonable request and with proper approval from relevant research and ethics entities. Requests to access the datasets should be directed to KS, kms424@cornell.edu.

ETHICS STATEMENT

The studies involving human participants were reviewed and approved by Cornell Institutional Review Board for Human Participant Research. The patients/participants provided their written informed consent to participate in this study.

AUTHOR CONTRIBUTIONS

RM: conceptualization, methodology, validation, formal analysis, investigation, data curation, writing – original draft, review and editing, and visualization. HT: conceptualization, methodology, validation, formal analysis, investigation, data curation, writing – review and editing, and visualization. W-ML: methodology, resources, and writing – review and editing. KS: conceptualization, methodology, formal analysis, investigation, resources, data curation, supervision, project administration, writing – review and editing, and funding acquisition. All authors contributed to the article and approved the submitted version.

FUNDING

This work was supported by an NIH NCRR grant [1S10RR025145] to the Cornell Magnetic Resonance Imaging Facilities, by the Intramural Research Program of NIA/NIH, and by the College of Arts and Sciences at Cornell University.

ACKNOWLEDGMENTS

We would like to thank Suyash Bhogawar, Bohan Li, Alyssa Phelps, Roy Proper, and Emily Qualls for their assistance with data collection. We would also like to thank Elizabeth Riley for her help with identification of the locus coeruleus, and Adam Anderson, Eve DeRosa, and Nathan Spreng for discussion of this work. A version of this manuscript has been placed on the BioRxiv preprint server as Moyal et al. (2022). Auditory Target Detection Enhances Visual Processing and Hippocampal Functional Connectivity (p. 2020.09.19.304881). bioRxiv. <https://doi.org/10.1101/2020.09.19.304881>.

SUPPLEMENTARY MATERIAL

The Supplementary Material for this article can be found online at: <https://www.frontiersin.org/articles/10.3389/fpsyg.2022.891682/full#supplementary-material>

REFERENCES

- Albers, A. M., Meindertsma, T., Toni, I., and de Lange, F. P. (2018). Decoupling of BOLD amplitude and pattern classification of orientation-selective activity in human visual cortex. *NeuroImage* 180, 31–40. doi: 10.1016/j.neuroimage.2017.09.046
- Aston-Jones, G., and Cohen, J. D. (2005). An integrative theory of locus coeruleus-norepinephrine function: adaptive gain and optimal performance. *Annu. Rev. Neurosci.* 28, 403–450.
- Aston-Jones, G., Rajkowski, J., Kubiak, P., and Alexinsky, T. (1994). Locus coeruleus neurons in monkey are selectively activated by attended cues in a vigilance task. *J. Neurosci.* 14, 4467–4480. doi: 10.1523/JNEUROSCI.14-07-04467.1994
- Bates, D., Mächler, M., Bolker, B., and Walker, S. (2015). Fitting linear mixed-effects models using lme4. *J. Statist. Soft. Articles* 67, 1–48.
- Bonnefond, M., Kastner, S., and Jensen, O. (2017). Communication between brain areas based on nested oscillations. *eneuro* 4:2. doi: 10.1523/ENEURO.0153-16.2017
- Bouret, S., and Sara, S. J. (2005). Network reset: a simplified overarching theory of locus coeruleus noradrenergic function. *Trends Neurosci.* 28, 574–582. doi: 10.1016/j.tins.2005.09.002
- Bretton-Provencher, V., and Sur, M. (2019). Active control of arousal by a locus coeruleus GABAergic circuit. *Nat. Neurosci.* 22, 218–228. doi: 10.1038/s41593-018-0305-z
- Broitman, A. W., and Swallow, K. M. (2020). The effects of encoding instruction and opportunity on the recollection of behaviourally relevant events. *Quart. J. Exp. Psychol.* 73, 711–725. doi: 10.1177/1747021819893676
- Carrasco, M. (2011). Visual attention: the past 25 years. *Vision Res.* 51, 1484–1525. doi: 10.1016/j.visres.2011.04.012
- Chadwick, M. J., Hassabis, D., and Maguire, E. A. (2011). Decoding overlapping memories in the medial temporal lobes using high-resolution fMRI. *Learn. Memory* 18, 742–746. doi: 10.1101/lm.023671.111
- Chadwick, M. J., Hassabis, D., Weiskopf, N., and Maguire, E. A. (2010). Decoding individual episodic memory traces in the human hippocampus. *Curr. Biol.* 20, 544–547. doi: 10.1016/j.cub.2010.01.053
- Chen, G., Saad, Z. S., Adelman, N. E., Leibenluft, E., and Cox, R. W. (2015). Detecting the subtle shape differences in hemodynamic responses at the group level. *Front. Neurosci.* 9:375. doi: 10.3389/fnins.2015.00375
- Chiu, Y. C., and Egner, T. (2015). Inhibition-induced forgetting results from resource competition between response inhibition and memory encoding processes. *J. Neurosci.* 35, 11936–11945. doi: 10.1523/JNEUROSCI.0519-15.2015
- Cisler, J. M., Bush, K., and Steele, J. S. (2014). A comparison of statistical methods for detecting context-modulated functional connectivity in fMRI. *NeuroImage* 84, 1042–1052. doi: 10.1016/j.neuroimage.2013.09.018
- Clewett, D., Gasser, C., and Davachi, L. (2020). Pupil-linked arousal signals track the temporal organization of events in memory. *Nat. Commun.* 11, 1–14. doi: 10.1038/s41467-020-17851-9
- Cox, R. W. (1996). AFNI: software for analysis and visualization of functional magnetic resonance neuroimages. *Comput. Biomed. Res.* 29, 162–173.
- Cox, R. W., Chen, G., Glen, D. R., Reynolds, R. C., and Taylor, P. A. (2017). FMRI clustering in AFNI: false-positive rates redux. *Brain Connect.* 7, 152–171. doi: 10.1089/brain.2016.0475
- Cox, R. W., and Hyde, J. S. (1997). Software tools for analysis and visualization of fMRI data. *NMR Biomed. Int. J. Dev. Dev. Appl. Magnet. Res. Vivo* 10, 171–178. doi: 10.1002/(sici)1099-1492(199706/08)10:4/5<171::aid-nbm453>3.0.co;2-l
- Dale, A. M., Fischl, B., and Sereno, M. I. (1999). Cortical surface-based analysis: I. segmentation and surface reconstruction. *NeuroImage* 9, 179–194. doi: 10.1006/nimg.1998.0395
- Diedrichsen, J., and Kriegeskorte, N. (2017). Representational models: a common framework for understanding encoding, pattern-component, and representational-similarity analysis. *PLoS Comput. Biol.* 13:e1005508. doi: 10.1371/journal.pcbi.1005508
- Ennis, M., Shipley, M. T., Aston-Jones, G., and Williams, J. T. (1998). Afferent control of nucleus locus coeruleus: differential regulation by “shell” and “core” inputs. *Adv. Pharmacol.* 42, 767–771. doi: 10.1016/s1054-3589(08)60860-1
- Fanselow, M. S., and Dong, H. W. (2010). Are the dorsal and ventral hippocampus functionally distinct structures? *Neuron* 65, 7–19. doi: 10.1016/j.neuron.2009.11.031
- Faul, F., Erdfelder, E., Lang, A. G., and Buchner, A. (2007). G* power 3: a flexible statistical power analysis program for the social, behavioral, and biomedical sciences. *Behav. Res. Methods* 39, 175–191. doi: 10.3758/bf03193146
- Fischl, B., Sereno, M. I., and Dale, A. M. (1999). Cortical surface-based analysis: II: inflation, flattening, and a surface-based coordinate system. *NeuroImage* 9, 195–207. doi: 10.1006/nimg.1998.0396
- Frank, L. E., Bowman, C. R., and Zeithamova, D. (2019). Differential functional connectivity along the long axis of the hippocampus aligns with differential role in memory specificity and generalization. *J. Cogn. Neurosci.* 31, 1958–1975. doi: 10.1162/jocn_a_01457
- Fries, P. (2005). A mechanism for cognitive dynamics: neuronal communication through neuronal coherence. *Trends Cogn. Sci.* 9, 474–480. doi: 10.1016/j.tics.2005.08.011
- Fries, P. (2015). Rhythms for cognition: communication through coherence. *Neuron* 88, 220–235. doi: 10.1016/j.neuron.2015.09.034
- Friston, K. J. (2011). Functional and effective connectivity: a review. *Brain Connect.* 1, 13–36.
- Gage, F. H., and Thompson, R. G. (1980). Differential distribution of norepinephrine and serotonin along the dorsal-ventral axis of the hippocampal formation. *Brain Res. Bull.* 5, 771–773. doi: 10.1016/0361-9230(80)90220-8
- Garrido, L., Vaziri-Pashkam, M., Nakayama, K., and Wilmer, J. (2013). The consequences of subtracting the mean pattern in fMRI multivariate correlation analyses. *Front. Neurosci.* 7:174. doi: 10.3389/fnins.2013.00174
- Gazzaley, A., Rissman, J., and D’Esposito, M. (2004). Functional connectivity during working memory maintenance. *Cogn. Affect. Behav. Neurosci.* 4, 580–599.
- Geib, B. R., Stanley, M. L., Dennis, N. A., Woldorff, M. G., and Cabeza, R. (2017). From hippocampus to whole-brain: the role of integrative processing in episodic memory retrieval. *Hum. Brain Mapp.* 38, 2242–2259. doi: 10.1002/hbm.23518
- Genovese, C. R., Lazar, N. A., and Nichols, T. (2002). Thresholding of statistical maps in functional neuroimaging using the false discovery rate. *NeuroImage* 15, 870–878. doi: 10.1006/nimg.2001.1037
- Gold, S., Christian, B., Arndt, S., Zeien, G., Cizadlo, T., Johnson, D. L., et al. (1998). Functional MRI statistical software packages: a comparative analysis. *Hum. Brain Mapp.* 6, 73–84. doi: 10.1002/(SICI)1097-0193(1998)6:2<aid-hbm10003e;3.0.CO;2-H
- Hatfield, M., McCloskey, M., and Park, S. (2016). Neural representation of object orientation: a dissociation between MVPA and repetition suppression. *NeuroImage* 139, 136–148. doi: 10.1016/j.neuroimage.2016.05.052
- Handwerker, D. A., Ollinger, J. M., and D’Esposito, M. (2004). Variation of BOLD hemodynamic responses across subjects and brain regions and their effects on statistical analyses. *NeuroImage* 21, 1639–1651.
- Haxby, J. V., Connolly, A. C., and Guntupalli, J. S. (2014). Decoding neural representational spaces using multivariate pattern analysis. *Ann. Rev. Neurosci.* 37, 435–456. doi: 10.1146/annurev-neuro-062012-170325
- Henson, R. N., Price, C. J., Rugg, M. D., Turner, R., and Friston, K. J. (2002). Detecting latency differences in event-related BOLD responses: application to words versus nonwords and initial versus repeated face presentations. *NeuroImage* 15, 83–97.
- Henson, R. N. A., and Rugg, M. D. (2003). Neural response suppression, haemodynamic repetition effects, and behavioural priming. *Neuropsychologia* 41, 263–270. doi: 10.1016/s0028-3932(02)00159-8
- Hirano, Y., Stefanovic, B., and Silva, A. C. (2011). Spatiotemporal evolution of the functional magnetic resonance imaging response to ultrashort stimuli. *J. Neurosci.* 31, 1440–1447. doi: 10.1523/JNEUROSCI.3986-10.2011
- Hsu, C. W., and Lin, C. J. (2002). A comparison of methods for multiclass support vector machines. *IEEE Trans. Neural Networks* 13, 415–425.
- Hu, S., Olulade, O., Castillo, J. G., Santos, J., Kim, S., Tamer, G. G., et al. (2010). Modeling hemodynamic responses in auditory cortex at 1.5 T using variable duration imaging acoustic noise. *NeuroImage* 49, 3027–3038. doi: 10.1016/j.neuroimage.2009.11.051
- Huettel, S. A., McKeown, M. J., Song, A. W., Hart, S., Spencer, D. D., Allison, T., et al. (2004). Linking hemodynamic and electrophysiological measures of

- brain activity: evidence from functional MRI and intracranial field potentials. *Cerebral Cortex* 14, 165–173. doi: 10.1093/cercor/bhg115
- Huang, G. B., and Learned-Miller, E. (2014). *Labeled Faces in the Wild: Updates and New Reporting Procedures*. Amherst, MA: Dept. Computer Science, Univ. Massachusetts Amherst, 14–13.
- Huang, G. B., Ramesh, M., Berg, T., and Learned-Miller, E. (2007). *Labeled Faces in the Wild: A Database for Studying Face Recognition in Unconstrained Environments*. Amherst: University of Massachusetts. .
- Jack, A. I., Shulman, G. L., Snyder, A. Z., McAvoy, M., and Corbetta, M. (2006). Separate modulations of human V1 associated with spatial attention and task structure. *Neuron* 51, 135–147. doi: 10.1016/j.neuron.2006.06.003
- Jefferies, L. N., and Di Lollo, V. (2019). Sudden events change old visual objects into new ones: a possible role for phasic activation of locus coeruleus. *Psychol. Sci.* 30, 55–64. doi: 10.1177/0956797618807190
- Jodoy, E., Chiang, C., and Aston-Jones, G. (1998). Potent excitatory influence of prefrontal cortex activity on noradrenergic locus coeruleus neurons. *Neuroscience* 83, 63–79. doi: 10.1016/s0306-4522(97)00372-2
- Johnson, J. A., and Zatorre, R. J. (2005). Attention to simultaneous unrelated auditory and visual events: behavioral and neural correlates. *Cerebral Cortex* 15, 1609–1620. doi: 10.1093/cercor/bhi039
- Joshi, S., Li, Y., Kalwani, R. M., and Gold, J. I. (2016). Relationships between pupil diameter and neuronal activity in the locus coeruleus, colliculi, and cingulate cortex. *Neuron* 89, 221–234. doi: 10.1016/j.neuron.2015.11.028
- Kempadoo, K. A., Mosharov, E. V., Choi, S. J., Sulzer, D., and Kandel, E. R. (2016). Dopamine release from the locus coeruleus to the dorsal hippocampus promotes spatial learning and memory. *Proc. Natl. Acad. Sci. U.S.A.* 113, 14835–14840. doi: 10.1073/pnas.1616515114
- Keren, N. I., Lozar, C. T., Harris, K. C., Morgan, P. S., and Eckert, M. A. (2009). In vivo mapping of the human locus coeruleus. *Neuroimage* 47, 1261–1267.
- Kim, K., Hsieh, L. T., Parvizi, J., and Ranganath, C. (2020). Neural repetition suppression effects in the human hippocampus. *Neurobiol. Learn. Memory* 2020:107269. doi: 10.1016/j.nlm.2020.107269
- Knapen, T., de Gee, J. W., Brascamp, J., Nuiten, S., Hoppenbrouwers, S., and Theeuwes, J. (2016). Cognitive and ocular factors jointly determine pupil responses under equiluminance. *PLoS One* 11:e0155574. doi: 10.1371/journal.pone.0155574
- Kundu, P., Inati, S. J., Evans, J. W., Luh, W. M., and Bandettini, P. A. (2012). Differentiating BOLD and non-BOLD signals in fMRI time series using multiecho EPI. *Neuroimage* 60, 1759–1770.
- Kundu, P., Brenowitz, N. D., Voon, V., Worbe, Y., Vértes, P. E., Inati, S. J., et al. (2013). Integrated strategy for improving functional connectivity mapping using multiecho fMRI. *Proc. Natl. Acad. Sci. U.S.A.* 110, 16187–16192. doi: 10.1073/pnas.1301725110
- Larsson, J., and Smith, A. T. (2012). fMRI repetition suppression: neuronal adaptation or stimulus expectation? *Cerebral Cortex* 22, 567–576. doi: 10.1093/cercor/bhr119
- Leclercq, V., Le Dantec, C. C., and Seitz, A. R. (2014). Encoding of episodic information through fast task-irrelevant perceptual learning. *Vision Res.* 99, 5–11. doi: 10.1016/j.visres.2013.09.006
- Lee, T. H., Greening, S. G., Ueno, T., Clewett, D., Ponzio, A., Sakaki, M., et al. (2018). Arousal increases neural gain via the locus coeruleus–noradrenergic system in younger adults but not in older adults. *Nat. Hum. Behav.* 2, 356–366.
- Length, R. (2020). *emmeans: Estimated Marginal Means, Aka Least-Squares Means. R Package Version 1.4.4*.
- Lewis, L. D., Setsompop, K., Rosen, B. R., and Polimeni, J. R. (2016). Fast fMRI can detect oscillatory neural activity in humans. *Proc. Natl. Acad. Sci. U.S.A.* 113, E6679–E6685. doi: 10.1073/pnas.1608117113
- Li, M., Han, Y., Aburn, M. J., Breakspear, M., Poldrack, R. A., Shine, J. M., et al. (2019). Transitions in information processing dynamics at the whole-brain network level are driven by alterations in neural gain. *PLoS Comput. Biol.* 15:e1006957. doi: 10.1371/journal.pcbi.1006957
- Li, X., Swallow, K., Chiu, M., De Rosa, E., and Anderson, A. K. (2018). Does the body give the brain an attentional boost? Examining the relationship between attentional and cardiac gating. *Biol. Psychol.* 139, 124–130.
- Mahmoudi, A., Takerkart, S., Regragui, F., Boussaoud, D., and Brovelli, A. (2012). Multivoxel pattern analysis for fMRI data: a review. *Comput. Math. Methods Med.* 2012:e961257. doi: 10.1155/2012/961257
- Makovski, T., Swallow, K. M., and Jiang, Y. V. (2011). Attending to unrelated targets boosts short-term memory for color arrays. *Neuropsychologia* 49, 1498–1505. doi: 10.1016/j.neuropsychologia.2010.11.029
- Makovski, T., Jiang, Y. V., and Swallow, K. M. (2013). How do observer's responses affect visual long-term memory? *J. Exp. Psychol. Learn. Memory Cogn.* 39:1097. doi: 10.1037/a0030908
- Miezin, F. M., Maccotta, L., Ollinger, J. M., Petersen, S. E., and Buckner, R. L. (2000). Characterizing the hemodynamic response: effects of presentation rate, sampling procedure, and the possibility of ordering brain activity based on relative timing. *Neuroimage* 11, 735–759. doi: 10.1006/nimg.2000.0568
- Moyal, R., and Edelman, S. (2019). Dynamic computation in visual thalamocortical networks. *Entropy* 21:500. doi: 10.3390/e21050500
- Moyal, R., Fekete, T., and Edelman, S. (2020). Dynamical emergence theory (DET): a computational account of phenomenal consciousness. *Minds Mach.* 2020, 1–21.
- Moyal, R., Turker, H., Luh, W.-M., and Swallow, K. M. (2022). Auditory target detection enhances visual processing and hippocampal functional connectivity (p. 2020.09.19.304881). *bioRxiv* [Preprint] doi: 10.1101/2020.09.19.304881
- Mulligan, N. W., Smith, S. A., and Spataro, P. (2016). The attentional boost effect and context memory. *J. Exp. Psychol. Learn. Memory Cogn.* 42:598. doi: 10.1037/xlm0000183
- Mulligan, N. W., and Spataro, P. (2015). Divided attention can enhance early-phase memory encoding: the attentional boost effect and study trial duration. *J. Exp. Psychol. Learn. Memory Cogn.* 41:1223. doi: 10.1037/xlm0000055
- Mulligan, N. W., Spataro, P., Rossi-Arnaud, C., and Wall, A. R. (2021). The attentional boost effect and source memory. *J. Exp. Psychol. Learn. Mem. Cogn.* doi: 10.1037/xlm0000990 [Epub ahead of print].
- Mumford, J. A., Turner, B. O., Ashby, F. G., and Poldrack, R. A. (2012). Deconvolving BOLD activation in event-related designs for multivoxel pattern classification analyses. *Neuroimage* 59, 2636–2643. doi: 10.1016/j.neuroimage.2011.08.076
- Murphy, P. R., O'connell, R. G., O'sullivan, M., Robertson, I. H., and Balsters, J. H. (2014). Pupil diameter covaries with BOLD activity in human locus coeruleus. *Hum. Brain Mapp.* 35, 4140–4154. doi: 10.1002/hbm.22466
- Nieuwenhuis, S., Aston-Jones, G., and Cohen, J. D. (2005). Decision making, the P3, and the locus coeruleus–norepinephrine system. *Psychol. Bull.* 131:510. doi: 10.1037/0033-2909.131.4.510
- Nobre, A. C., and van Ede, F. (2018). Anticipated moments: temporal structure in attention. *Nat. Rev. Neurosci.* 19:34.
- Pascucci, D., and Turatto, M. (2013). Immediate effect of internal reward on visual adaptation. *Psychol. Sci.* 24, 1317–1322. doi: 10.1177/0956797612469211
- Pedregosa, F., Varoquaux, G., Gramfort, A., Michel, V., Thirion, B., Grisel, O., et al. (2011). Scikit-learn: machine learning in python. *J. Mach. Learn. Res.* 12, 2825–2830. doi: 10.1080/13696998.2019.1666854
- Persson, J., Stening, E., Nordin, K., and Söderlund, H. (2018). Predicting episodic and spatial memory performance from hippocampal resting-state functional connectivity: evidence for an anterior–posterior division of function. *Hippocampus* 28, 53–66. doi: 10.1002/hipo.22807
- Pihlajamäki, M., O'Keefe, K., O'Brien, J., Blacker, D., and Sperling, R. A. (2011). Failure of repetition suppression and memory encoding in aging and Alzheimer's disease. *Brain Imaging Behav.* 5, 36–44. doi: 10.1007/s11682-010-9110-3
- Poch, C., and Campo, P. (2012). Neocortical-hippocampal dynamics of working memory in healthy and diseased brain states based on functional connectivity. *Front. Hum. Neurosci.* 6:36. doi: 10.3389/fnhum.2012.00036
- Polimeni, J. R., and Lewis, L. D. (2021). Imaging faster neural dynamics with fast fMRI: a need for updated models of the hemodynamic response. *Prog. Neurobiol.* 2021:102174. doi: 10.1016/j.pneurobio.2021.102174
- Poppenk, J., Evensmoen, H. R., Moscovitch, M., and Nadel, L. (2013). Long-axis specialization of the human hippocampus. *Trends Cogn. Sci.* 17, 230–240.
- R Core Team (2013). *R: A Language and Environment for Statistical Computing*. Vienna: R Foundation for Statistical Computing.
- Ranganath, C., Heller, A., Cohen, M. X., Brozinsky, C. J., and Rissman, J. (2005). Functional connectivity with the hippocampus during successful memory formation. *Hippocampus* 15, 997–1005. doi: 10.1002/hipo.20141
- Rissman, J., Gazzaley, A., and D'Esposito, M. (2004). Measuring functional connectivity during distinct stages of a cognitive task. *Neuroimage* 23, 752–763. doi: 10.1016/j.neuroimage.2004.06.035

- Rohenkohl, G., Coull, J. T., and Nobre, A. C. (2011). Behavioural dissociation between exogenous and endogenous temporal orienting of attention. *PLoS One* 6:e14620. doi: 10.1371/journal.pone.0014620
- Saalmann, Y. B., and Kastner, S. (2011). Cognitive and perceptual functions of the visual thalamus. *Neuron* 71, 209–223. doi: 10.1016/j.neuron.2011.06.027
- Sara, S. J. (2009). The locus coeruleus and noradrenergic modulation of cognition. *Nat. Rev. Neurosci.* 10, 211–223. doi: 10.1038/nrn2573
- Sara, S. J. (2015). Locus coeruleus in time with the making of memories. *Curr. Opin. Neurobiol.* 35, 87–94. doi: 10.1016/j.conb.2015.07.004
- Schonberg, T., Bakkour, A., Hover, A. M., Mumford, J. A., Nagar, L., Perez, J., et al. (2014). Changing value through cued approach: an automatic mechanism of behavior change. *Nat. Neurosci.* 17, 625–630. doi: 10.1038/nn.3673
- Schott, B. H., Wüstenberg, T., Wimber, M., Fenker, D. B., Zierhut, K. C., Seidenbecher, C. I., et al. (2013). The relationship between level of processing and hippocampal–cortical functional connectivity during episodic memory formation in humans. *Hum. Brain Mapp.* 34, 407–424. doi: 10.1002/hbm.21435
- Seidl, K. N., Peelen, M. V., and Kastner, S. (2012). Neural evidence for distracter suppression during visual search in real-world scenes. *J. Neurosci.* 32, 11812–11819. doi: 10.1523/JNEUROSCI.1693-12.2012
- Servan-Schreiber, D., Printz, H., and Cohen, J. D. (1990). A network model of catecholamine effects: gain, signal-to-noise ratio, and behavior. *Science* 249, 892–895. doi: 10.1126/science.2392679
- Shine, J. M., Aburn, M. J., Breakspear, M., and Poldrack, R. A. (2018). The modulation of neural gain facilitates a transition between functional segregation and integration in the brain. *Elife* 7:e31130. doi: 10.7554/eLife.31130
- Silver, M. A., Ress, D., and Heeger, D. J. (2007). Neural correlates of sustained spatial attention in human early visual cortex. *J. Neurophysiol.* 97, 229–237. doi: 10.1152/jn.00677.2006
- Singer, W. (2013). Cortical dynamics revisited. *Trends Cogn. Sci.* 17, 616–626. doi: 10.1016/j.tics.2013.09.006
- Spataro, P., Mulligan, N. W., and Rossi-Arnaud, C. (2013). Divided attention can enhance memory encoding: the attentional boost effect in implicit memory. *J. Exp. Psychol. Learn. Memory Cogn.* 39:1223. doi: 10.1037/a0030907
- Summerfield, C., Trittschuh, E. H., Monti, J. M., Mesulam, M. M., and Egner, T. (2008). Neural repetition suppression reflects fulfilled perceptual expectations. *Nat. Neurosci.* 11:1004.
- Suykens, J. A., and Vandewalle, J. (1999). Least squares support vector machine classifiers. *Neural Proc. Lett.* 9, 293–300.
- Swallow, K. M., and Atir, S. (2019). The role of value in the attentional boost effect. *Quart. J. Exp. Psychol.* 72, 523–542. doi: 10.1177/1747021818760791
- Swallow, K. M., and Jiang, Y. V. (2010). The attentional boost effect: transient increases in attention to one task enhance performance in a second task. *Cognition* 115, 118–132. doi: 10.1016/j.cognition.2009.12.003
- Swallow, K. M., and Jiang, Y. V. (2012). The role of timing in the attentional boost effect. *Attent. Percept. Psychophys.* 73, 389–404. doi: 10.3758/s13414-010-0045-y
- Swallow, K. M., and Jiang, Y. V. (2013). Attentional load and attentional boost: a review of data and theory. *Front. Psychol.* 4:274. doi: 10.3389/fpsyg.2013.00274
- Swallow, K. M., and Jiang, Y. V. (2014). The attentional boost effect really is a boost: evidence from a new baseline. *Attent. Percept. Psychophys.* 76, 1298–1307.
- Swallow, K. M., Jiang, Y. V., and Riley, E. B. (2019). Target detection increases pupil diameter and enhances memory for background scenes during multi-tasking. *Sci. Rep.* 9, 1–13. doi: 10.1038/s41598-019-41658-4
- Swallow, K. M., Makovski, T., and Jiang, Y. V. (2012). Selection of events in time enhances activity throughout early visual cortex. *J. Neurophysiol.* 108, 3239–3252. doi: 10.1152/jn.00472.2012
- Takeuchi, T., Duzsikiewicz, A. J., Sonneborn, A., Spooner, P. A., Yamasaki, M., Watanabe, M., et al. (2016). Locus coeruleus and dopaminergic consolidation of everyday memory. *Nature* 537, 357–362. doi: 10.1038/nature19325
- Tian, P., Teng, I. C., May, L. D., Kurz, R., Lu, K., Scadeng, M., et al. (2010). Cortical depth-specific microvascular dilation underlies laminar differences in blood oxygenation level-dependent functional MRI signal. *Proc. Natl. Acad. Sci. U.S.A.* 107, 15246–15251. doi: 10.1073/pnas.1006735107
- Toh, Y. N., and Lee, V. G. (2022). Response, rather than target detection, triggers the attentional boost effect in visual search. *J. Exp. Psychol. Hum. Percept. Perform.* 48:77. doi: 10.1037/xhp0000977
- Turker, H. B., Riley, E., Luh, W. M., Colcombe, S. J., and Swallow, K. M. (2021). Estimates of locus coeruleus function with functional magnetic resonance imaging are influenced by localization approaches and the use of multi-echo data. *NeuroImage* 236:118047. doi: 10.1016/j.neuroimage.2021.118047
- Turker, H. B., and Swallow, K. M. (2019). Attending to behaviorally relevant moments enhances incidental relational memory. *Memory Cogn.* 47, 1–16. doi: 10.3758/s13421-018-0846-0
- van der Wel, P., and van Steenbergen, H. (2018). Pupil dilation as an index of effort in cognitive control tasks: a review. *Psychon. Bull. Rev.* 25, 2005–2015. doi: 10.3758/s13423-018-1432-y
- Wagatsuma, A., Okuyama, T., Sun, C., Smith, L. M., Abe, K., and Tonegawa, S. (2018). Locus coeruleus input to hippocampal CA3 drives single-trial learning of a novel context. *Proc. Natl. Acad. Sci. U.S.A.* 115, E310–E316. doi: 10.1073/pnas.1714082115
- Walther, A., Nili, H., Ejaz, N., Alink, A., Kriegeskorte, N., and Diedrichsen, J. (2016). Reliability of dissimilarity measures for multi-voxel pattern analysis. *NeuroImage* 137, 188–200. doi: 10.1016/j.neuroimage.2015.12.012
- Wang, C. A., and Munoz, D. P. (2015). A circuit for pupil orienting responses: implications for cognitive modulation of pupil size. *Curr. Opin. Neurobiol.* 33, 134–140. doi: 10.1016/j.conb.2015.03.018
- Ward, E. J., Chun, M. M., and Kuhl, B. A. (2013). Repetition suppression and multi-voxel pattern similarity differentially track implicit and explicit visual memory. *J. Neurosci.* 33, 14749–14757. doi: 10.1523/JNEUROSCI.4889-12.2013
- Willenbockel, V., Sadr, J., Fiset, D., Horne, G. O., Gosselin, F., and Tanaka, J. W. (2010). Controlling low-level image properties: the SHINE toolbox. *Behav. Res. Methods* 42, 671–684. doi: 10.3758/BRM.42.3.671
- Xiang, Y., Mottaghi, R., and Savaresi, S. (2014). “Beyond pascal: a benchmark for 3d object detection in the wild,” in *Proceeding of the IEEE Winter Conference On Applications Of Computer Vision*, (IEEE), 75–82.
- Yebrá, M., Galarza-Vallejo, A., Soto-Leon, V., Gonzalez-Rosa, J. J., de Berker, A. O., Bestmann, S., et al. (2019). Action boosts episodic memory encoding in humans via engagement of a noradrenergic system. *Nat. Commun.* 10, 1–12. doi: 10.1038/s41467-019-11358-8
- Zhang, Y., Meyers, E. M., Bichot, N. P., Serre, T., Poggio, T. A., and Desimone, R. (2011). Object decoding with attention in inferior temporal cortex. *Proc. Natl. Acad. Sci. U.S.A.* 108, 8850–8855. doi: 10.1073/pnas.1100999108
- Zweynert, S., Pade, J. P., Wüstenberg, T., Sterzer, P., Walter, H., Seidenbecher, C. I., et al. (2011). Motivational salience modulates hippocampal repetition suppression and functional connectivity in humans. *Front. Hum. Neurosci.* 5:144. doi: 10.3389/fnhum.2011.00144

Conflict of Interest: The authors declare that the research was conducted in the absence of any commercial or financial relationships that could be construed as a potential conflict of interest.

Publisher's Note: All claims expressed in this article are solely those of the authors and do not necessarily represent those of their affiliated organizations, or those of the publisher, the editors and the reviewers. Any product that may be evaluated in this article, or claim that may be made by its manufacturer, is not guaranteed or endorsed by the publisher.

Copyright © 2022 Moyal, Turker, Luh and Swallow. This is an open-access article distributed under the terms of the Creative Commons Attribution License (CC BY). The use, distribution or reproduction in other forums is permitted, provided the original author(s) and the copyright owner(s) are credited and that the original publication in this journal is cited, in accordance with accepted academic practice. No use, distribution or reproduction is permitted which does not comply with these terms.